CHARACTERIZATION OF FRACTURE TOUGHNESS IN AMORPHOUS DIAMOND LIKE CARBON THIN FILMS AND COATINGS

by

RONAKSINH PARMAR

Presented to the Faculty of the Graduate School of

The University of Texas at Arlington in Partial Fulfillment

of the Requirements

for the Degree of

MASTER OF SCIENCE IN MATERIALS SCIENCE & ENGINEERING

THE UNIVERSITY OF TEXAS AT ARLINGTON

AUGUST 2015

Acknowledgement

Though only my name appears on the cover of this dissertation, but many people have contributed to its production. This thesis would not have been possible without the guidance of my advisor, committee members, help from my friends, support from my family and my roommates

Foremost, I would like to express my deepest gratitude to my advisor, Dr. Efstathios I. Meletis, for his excellent guidance, motivation and support. His guidance helped me throughout my research work and writing of this thesis. He provided me with a excellent atmosphere to carry out my research in my own way and financially supporting my research. I could not have imagined a better advisor and mentor for my Graduate education. Beside my advisor, a special thank goes to Dr. Reza Mirshams from University of North Texas for his extraordinary assistance in initial stage of my research, and my committee: Dr. Fuqiang Liu & Dr. Harry F. Tibbals for participating in my final defense and giving their valuable suggestions and guidance.

My sincere thanks to my colleagues Randall Kelton & Minghui Zhang, for constant support with nanoindentation testing and for additional help in lab work. I would like to thank Dr. Ramazan Karslioglu, Supraja Venkatakamakshi Giddaluri and Snigdha Rashinkar for their valuable suggestions and ideas for my thesis. Additional thanks to all Surface and Nano Engineering Laboratory (SANEL) group students for their suggestions.

Finally, I take this opportunity to express a profound appreciation from depth of my heart to my father and my two elder sisters for their love, and continuous support for my education in United States, and I would like to dedicate this thesis in the memory of my late mother Indraba Parmar. And last but not least I would like to thank all my friends, roommates and well-wishers for their constant inspiration and support.

I owe my gratitude to all these people who have made this dissertation possible and due to whom my graduate experience has been one that I will cherish forever.

JULY 23, 2015

Abstract

CHARACTERIZATION OF FRACTURE TOUGHNESS IN

AMORPHOUS DIAMOND LIKE CARBON

THIN FILMS AND COATINGS

RONAKSINH PARMAR, M.S.

The University of Texas at Arlington, 2015

Supervising Professor: Efstathios I. Meletis

Any material containing a crack when subjected to a certain amount of load, will eventually fail. This failure of material can be either time consuming (ductile) or instant (brittle) depending on the type of material and amount of load applied. For one to be able to study fracture toughness, it is important to study the material's failure rate and how long it can withstand load without failure once a crack has been initiated. Ductile materials demonstrate high fracture toughness while brittle materials show lower fracture toughness and fail instantly once a crack has been initiated.

Characterization of fracture toughness in bulk materials is easy and well established. However, it becomes difficult when dealing with brittle thin films. As the coating thickness decreases below ~1 μm, it becomes increasingly difficult to evaluate fracture toughness using conventional methods. Bulk materials can also be machined easily for making test specimen but Diamond like Carbon (DLC) thin films cannot be synthesized in bulk.

Micro and nano-indentation techniques are proposed for cases where conventional tension test and impact test fails to evaluate fracture toughness. Indentation techniques are very well developed for hardness measurement in all types of materials.

This paper is focusing towards characterization of fracture toughness in brittle (100) single crystal Silicon (Si) and DLC films coated on Si substrate. Such DLC thin films are designed to enhance thermal, oxidation, corrosion and mechanical resistance of substrate materials. Though sometimes service lifetime of such coatings in applications is limited by their fracture resistance or fracture toughness. Indentation is an easy, inexpensive, and non-destructive method for mechanical characterization for small volume of material. Such indentation is made using three sided or four sided diamond tip like, Vickers and cube-corner. Fracture toughness can be evaluated by analyzing the radial cracks formed by this indentation.

Presence of DLC coating reduces the radial crack length compared to crack length observed in uncoated Si. Different indentation models are used for characterization of fracture toughness in DLC thin films and Si wafer. It is found that the strain energy release model is most appropriate for evaluating fracture toughness in these films. The most challenging part of this research was to understand the effect of substrate on thin films and a way to evaluate the fracture toughness of thin films without the influence of substrate material.

Table of Contents

Acknowledgement iii

Abstract v

Table of Contents vii

List of Illustrations ix

List of Tables xi

Chapter 1 Introduction 1

Chapter 2 Objective 3

Chapter 3 Literature Review 4

3.1 Introduction to Indentation 4

3.2 Principles of Indentation 6

3.2.1 Elastic Contact Mechanics 6

3.2.2 Elastic-Plastic Contact Mechanics 9

3.2.3 Applications 10

3.3 Types of Indenter Tip 13

3.4 Types of Cracks 15

3.5 Fracture Toughness 16

3.6 Fracture in Thin Films 17

3.7 Fracture Toughness Models 19

3.7.1 For Vickers Indentation with Half-penny Crack 19

3.7.2 For Vickers Indentation with Palmqvist Crack 21

3.7.3 For Cube-corner Indentation 21

Chapter 4 Experimental Procedure 25

Chapter 5 Results and Discussion 27

5.1 Calibration Sample Analysis 27

5.1.1 Calibration Check for Microhardness Testing 27
5.1.2 Calibration Check for Nanoindentation Testing. 28
5.2 DLC Coating Thickness Measurement using Profilometer 30
5.2.1 Profilometer analysis of 0.4 μm DLC 30
5.2.2 Profilometer analysis of 0.85 μm DLC 31
5.3 Fracture Toughness Measurement of (100) Single Crystal Si using Vickers Indenter 31
5.4 Fracture Toughness Measurement of 0.4 μm DLC using Vickers Indenter 37
5.5 Fracture Toughness Measurement of 0.85 μm DLC using Vickers Indenter 43
5.6 Fracture Toughness Measurement of (100) Single Crystal Si using Cube-corner Indenter 48
5.7 Fracture Toughness Measurement using Work Approach Model 52
5.8 Fracture Toughness Measurement using Energy Release Model 56
5.9 Summary of Results 58
Chapter 6 Conclusion 59
References 60
Biographical Information 63

List of Illustrations

Figure 3-1 Cracks generated due to rupture of crystal bonds 6

Figure 3-2 Schematic of contact between spherical rigid indenter and flat specimen 6

Figure 3-3 Schematic of contact between conical rigid indenter and flat specimen 8

Figure 3-4 Schematic of typical indenter load vs. indenter displacement curve 11

Figure 3-5 (a) Vickers indenter tip under optical microscope, (b) Cube-corner indenter tip under SEM 14

Figure 3-6 (a) Radial/ Palmqvist crack, (b) Lateral crack, (c) Median crack, (d) Half-penny crack (e) Cross-section of Half-Penny Crack and (f) Cross-section of Radial/Palmqvist crack 15

Figure 3-7 (a) Impression of Vickers indentation and (b) Impression of cube-corner indentation on specimen surface 16

Figure 3-8 Schematic of various stages of indentation fracture in film/substrate system 18

Figure 3-9 (a) Peak load (Fm), unloading work (Wu) and total loading work (Wt), (b) length of radial crack c 23

Figure 3-10 Schematic of load-displacement curve, showing a step/plateau during loading cycle 24

Figure 5-1 Load vs. Hardness curve for standard steel sample 27

Figure 5-2 Nanoindentation analysis of standard fused Quartz sample 29

Figure 5-3 Coating thickness measurement using Profilometer for 0.4μm DLC thin film 30

Figure 5-4 Coating thickness measurement using Profilometer for 0.85μm DLC thin film 31

Figure 5-5 Graph of load vs. fracture toughness for different half-penny crack models, measured on single crystal Si 33

Figure 5-6 Graphs of load vs. hardness for single crystal Si 34
Figure 5-7 Vickers indentation image at 500X magnification on Si surface, at load (a) 10 gf, (b) 25 gf, (c) 50 gf, (d) 100 gf, (e) 200 gf and (f) 200 gf 35
Figure 5-8 Graph of load vs. fracture toughness for different half-penny crack models, measured on 0.4 μm DLC thin film 39
Figure 5-9 Graphs of load vs. hardness for 0.4 μm DLC thin film 40
Figure 5-10 Vickers indentation image at 500x magnification on 0.4 μm DLC thin film surface, at load (a) 50 gf, (b) 100 gf, (c) 200 gf, (d) 300 gf, (e) 500 gf and (f) 500 gf..... 41
Figure 5-11 Graph of load vs. fracture toughness for different half-penny crack models, measured on 0.85 μm DLC thin film 45
Figure 5-12 Graphs of load vs. hardness for 0.85 μm DLC thin film 46
Figure 5-13 Vickers indentation image at 500x magnification on 0.85 μm DLC thin film, at load (a) 25 gf, (b) 50 gf, (c) 100 gf, (d) 200 gf, (e) 300 gf and (f) 500 gf..... 47
Figure 5-14 Graph of load vs. fracture toughness in single crystal Si using different model of cube-corner indenter 50
Figure 5-15 Nanoindentation images made by cube-corner indenter at load (a) 2500 μN, (b) 5000 μN, (c) 6000 μN, (d) 7000 μN, (e) 8500 μN and (f) 9500 μN 51
Figure 5-16 Graph of load vs. fracture toughness, measured using work approach model for single crystal Si 54
Figure 5-17 Cube-corner indentation on 0.4 μm DLC thin film 56
Figure 5-18 Load vs. Displacement curve for 0.4 μm DLC thin film 57

List of Tables

Table 3-1Different types of indenter tip and there summary.....13

Table 5-1 Microhardness testing result for standard steel block of 776 HV hardness 27

Table 5-2 Fracture toughness measurement using half-penny crack models for (100) single crystal Si using Vickers indenter.....32

Table 5-3 Fracture toughness measurement using half-penny crack models for 0.4 µm DLC using Vickers indenter 38

Table 5-4 Fracture toughness measurement using half-penny crack models for 0.85 µm DLC using Vickers indenter 44

Table 5-5 Fracture toughness measurement of (100) single crystal Si using cube-corner indenter 49

Table 5-6 Fracture toughness measurement using work approach method in (100) single crystal Si.....53

Table 5-7 Fracture toughness measurement using strain energy release model 57

Chapter 1

Introduction

DLC thin films are metastable forms of amorphous carbon with significant sp^3 bonding displaying diamond-like properties. They have widespread applications, ranging from protective coatings in areas like optical windows, magnetic storage disks, and automobile parts to micro-electromechanical devices (MEMs) [1]. The development of DLC coatings was motivated by the engineering need to improve thermal, oxidation, corrosion, and mechanical properties for a host of substrate materials. In many applications, the performance and service life of such DLC coating is limited by the fracture resistance or fracture toughness of the coating material. Frequently, the new and novel materials produced by coatings cannot be synthesized in bulk. Hence, fracture toughness evaluation using common bulk materials' fracture techniques is not possible. In such circumstances it would be advisable to devise a simple method to evaluate the fracture toughness of DLC thin films such that, it could be evaluated while attached to the substrate [2].

During the last 25 years, several indentation techniques have been developed which allow fracture toughness determination. By measuring the crack lengths generated on the edge of indent during controlled indentation, fracture toughness can be evaluated. Multiple models of fracture toughness have been proposed which yield different results for different types of material [3].

In this research work initial approach was made to study a brittle substrate; pure single crystal Si. Pure Si is a tetravalent metalloid commonly used in electronics due to its semi-conductive property. It is generally doped with traces of boron or phosphorous to enhance its electrical properties. The Si sliced to thin wafer is mainly used in digital electronic circuits.

Si wafer is coated with DLC thin films. Two samples of DLC coating are prepared using Magnetron Sputtering, one with a coating thickness of 0.4 μm and a second with thickness of 0.85 μm. Fracture toughness measurements are carried out on this thin film samples using two indentation technique, LECO LM-Series microindentation hardness testing and Hysitron Ubi 1 nanoindenter.

LECO microindentation hardness tester is designed to achieve indentation with varying load rage of 10 gf to 1 kgf. It has a attach microscope with measuring scale for measurement and imaging of indentation at 500X magnification. Knoop and Vickers indenters, made of diamond are used for indenting the specimen surface. For current application Vickers indenter is used, it produces much larger radial cracks without causing chipping in the specimen surface makes it excel in: (i) improving the accuracy of the measurement of radial crack lengths; (ii) reducing the influence of grain sizes in coarser materials; (iii) locating indents efficiently [4]. Cracks generated under Vickers tip follow the axis of the diagonal of the indent impression which decreases the secondary crack growth in brittle material, allowing measuring more accurately [5].

In Hysitron Ubi 1 (nanoindenter), during the indentation analysis, load and depth are constantly measured to evaluate elastic modulus and hardness of small volume. Nanoindenter uses different tip shapes such as Conical, Berkovich, Spherical and Cube-corner tip for indentation. Nanoindentation and Atomic Force Microscopy (AFM) are combined in Ubi 1 for mechanical characterization of brittle materials or thin films and imaging the indentation in detail. Current research uses cube-corner tip as it can exert higher stress concentration compared to other indenter tip. It is ideal for measuring the mechanical properties at small displacement for thin film because exceeding 10% of thickness will show influence of substrate in the mechanical characterization of thin films.

Chapter 2

Objective

The goal of current study was to measure the fracture toughness of DLC thin films, deposited by Magnetron Sputtering. These DLC thin films are coated on Si wafer and the thickness is less than 1 μm.

The main objective of research work was;

I. To characterize the fracture toughness in DLC film without influence of substrate material.
II. To characterize the fracture toughness in brittle substrates and brittle materials.
III. Study different models of fracture toughness based on crack geometry.

Chapter 3

Literature Review

With advancing age, there are numerous applications in the world that utilize thin films for their mechanical, chemical or electrical properties. These increases in demand of thin films originated the rise of thin films research. These thin films have various applications ranging from microelectronics components, medical implants, and surface protection to automotive industries. Among all thin films, one of the most fascinating and most researched is DLC. DLC films are very interesting because of their vast applications. DLC is like a layer of pure Carbon in sp^3 bonding state, similar to diamond deposited on a substrate to enhance the surface mechanical resistance, corrosion resistance, and for surface appealing. It can also be used as a thermally conductive layer in electrical devices and could be doped to produce semi-conductivity [7]. For mechanical characterization of such DLC films the most suitable method studied is indentation technique.

3.1 Introduction to Indentation

Indentation long has been considered a very reliable technique for hardness measurement. Indentation is a simple method that consists essentially of touching the material of interest, of unknown mechanical properties, with a material of known mechanical properties. The technique has its origins in Moh's hardness scale of 1822. In which materials that are able to leave a permanent scratch in another were ranked harder material with diamond assigned the maximum value of 10 on the scale [6]. Upon indenting specimen surface with three sided or four sided diamond indenter results in crack formation on the surface, mainly in peripheral region of indent. These cracks can be used to measure the fracture toughness of the brittle material and thin film materials.

During any indentation process the load and corresponding displacement response is recorded and plotted. By considering the indenter's tip shape, geometry and monitoring the steady load increase, during the indentation, we can measure indentation depth, hardness and modules of elasticity of any material. Measuring the average crack length achieved at maximum loading we can also characterize fracture toughness of a given material. During loading, tensile stress are induced in the specimen material as the radius of the plastic zone increases. Upon unloading, additional stress arises as the elastically strained material outside the plastic zone attempts to resume its original shape but is prevented from doing so by the permanent deformation associated with the plastic zone [8]. Radial cracks are thought to emanate from the indent as a result of residual tensile stresses that develop during unloading [9].

Indentation method is expanding cavity mode, in which three zones are generated during the loading process; core, plastic zone and elastic zone. The first zone is the core, generated when pyramidal indenter starts the penetration of specimen. In such, residual stresses remain when unloading. Plastic zone is the second and is the zone that deforms permanently after loading because of the residual stresses in the first zone. The last is the elastic zone, after unloading this return to its original shape. This model is shown in figure 3-1.

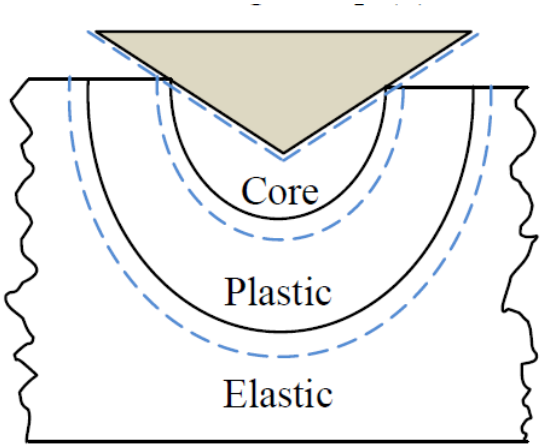

Figure 3-1 Cracks generated due to rupture of crystal bonds

3.2 Principles of Indentation

In order to study indentation, the principles of contact mechanics must be studied. Contact mechanics deal with the interaction between two solid objects. It is generally divided into elastic contact and elastic-plastic contact. A brief overview of these principles follows.

3.2.1 Elastic Contact Mechanics

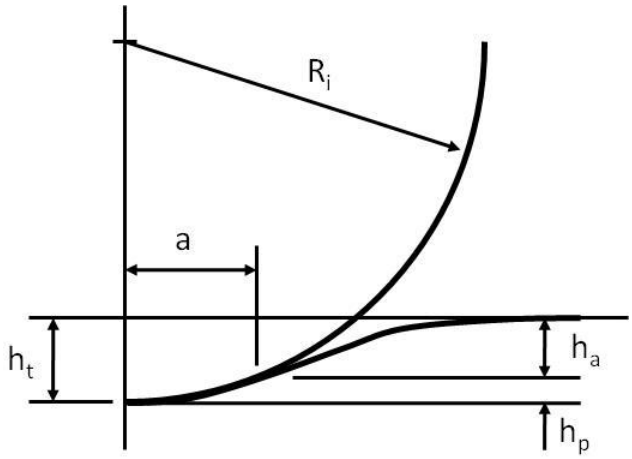

Figure 3-2 Schematic of contact between spherical rigid indenter and flat specimen

Consider a rigid spherical indenter of radius R_i in contact with a flat specimen as shown in Figure 3-2. Hence radius of the circle of contact a for an indentation at load P can be found as: [10]

$$a^3 = \frac{3PR_i}{4\mathrm{E}^*} \tag{3.1}$$

where the reduced modulus E^*, is a combination of indenter and specimen modulus:

$$\frac{1}{\mathrm{E}^*} = \frac{1-\nu^2}{E} + \frac{1-\nu'^2}{E'} \tag{3.2}$$

where the primed terms apply to the indenter properties.

For deformation with radius r and contact depth h on the specimen free surface in the vicinity of indenter at load P is given by:

$$h = \frac{3P}{8\mathrm{E}^* a}\left(2 - \frac{r^2}{a^2}\right) \quad r \le a \tag{3.3}$$

It can be shown from Equation (3.3) that the depth of the circle of contact beneath the specimen free surface is half of the total elastic displacement, i.e. $h_a = h_p = \mathrm{h_t}/2$

The mean contact pressure P_m, often referred to as the indentation stress, is given by the indenter load divided by the contact area and is a useful normalizing parameter:

$$P_m = P/\pi a^2 \tag{3.4}$$

Combining equation (3.1) & (3.4) we obtain:

$$P_m = \left(\frac{4E^*}{3\pi}\right)\frac{a}{r} \tag{3.5}$$

The mean contact pressure P_m and quantity a/r are referred as indentation stress and strain, respectively. This functional relation between them in equation (3.5) foreshadows the existence of stress-strain response, which is similar to that observed in conventional uniaxial tension and compression test.

Indentation exerts localized stress field on the specimen's surface, resulting in valuable information such as elastic-plastic property of the test based on stress-strain relationship. Generally this information cannot be obtained from uniaxial tension or compression tests.

In indentation testing the most common type of indenters are spherical and pyramidal indenters. The most common type of pyramidal indenter is four sided Vickers and three sided cube-corner indenter

Now, consider a conical indenter as shown in Figure 3-3. The radius of contact a for a given indentation load P is given by [12]:

$$P = \frac{\pi a}{2} E^* a \cot \alpha \tag{3.6}$$

and the deformation of the free surface is given by

$$h = \left(\frac{\pi}{2} - \frac{r}{a}\right) a \cot \alpha \quad r \leq a \tag{3.7}$$

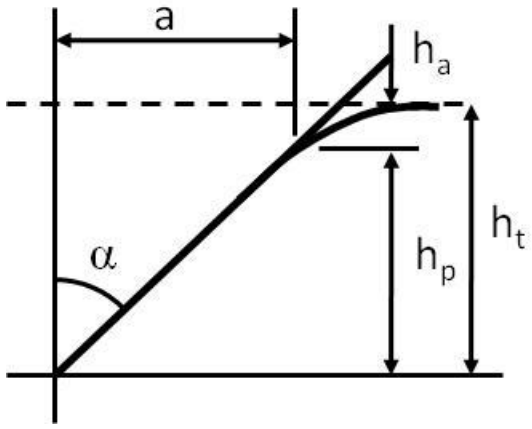

Figure 3-3 Schematic of contact between conical rigid indenter and flat specimen

Contact occurs at h_p (depth of circle of contact) is equal to the quantity $a \cot \alpha$.

Combining Equation (3.6) and Equation (3.7) at $r = 0$ yields:

$$P = \frac{2E \tan \alpha}{\pi} {h_t}^2 \tag{3.8}$$

with h_t being the total indentation depth of the indenter tip. The mean contact pressure for a conical indenter is again given by Equation (3.4). Combining equation (3.4) and (3.8) yields:

$$P_m = \frac{1}{2} E \cot \alpha \tag{3.9}$$

which is constant for a given indenter and specimen. This means that the indentation has geometric similarity and it is not possible to scale the indentation without external reference. This is dissimilar from a spherical indenter, thus care must be taken when using spherical indenters to maintain a constant indentation strain.

3.2.2 Elastic-Plastic Contact Mechanics

Indentation on specimen generally results in both elastic and plastic deformations. In brittle materials, plastic deformation most commonly occurs with pointed indenter such as Vickers and in ductile materials, plasticity may be readily induced with a blunt indenter such as spherical. This caused considerable debate on the meaning of hardness. Early methods, such as the scratch test used by Moh's', involved too many variables to give a good meaning to hardness. It wasn't until Hertz [17, 19] postulated that hardness was the least amount of pressure needed to produce a permanent indent at the center of the contact area that a manageable definition emerged. Later works have mostly been refinements of this idea.

It has been experimentally shown that the hardness number, H, is related to the mean contact pressure P_m at which there is no increase with increase in indenter load. At this limit, the hardness number is given directly by the mean contact pressure for hardness methods that use the projected contact area such as nano or micro indentation.

The specimen's yield stress σ_y has been experimentally shown to be directly proportional to the hardness and can be expressed as:

$$H \approx C\sigma_y \tag{3.10}$$

where $C \approx 3$ for materials with a large ratio of $\frac{E}{\sigma_y}$ such as metals, and

$C \approx 1.5$ for materials with a low $\frac{E}{\sigma_y}$ ratio such as glass.

The hardness of a material is related to mean contact pressure P_m beneath the indenter at a limiting condition of compression. Valuable information about elastic-plastic deformation is obtained by plotting spherical indentation stress (σ_y) vs. indentation strain (a/r). The indentation stress-strain response of an elastic-plastic solid can be divided into three regimes,

1) $P_m < 1.1\sigma_y$ gives full elastic response, no permanent impression is found after indentation.

2) $1.1\sigma_y < P_m < C\sigma_y$ gives plastic deformation beneath the surface but it is constrained by surrounding elastic material, where C is constant based on material and indenter geometry.

3) $P_m = C\sigma_y$ extends plastic region to the surface of specimen and continue to grow in size such that contact area increases without an increase in mean contact pressure P_m.

3.2.3 Applications

Since a typical indentation has both elastic and plastic deformations, the calculations of the hardness and the elastic modulus of a specimen is not necessarily straight forward. Figure 3-4 shows a typical indenter load versus displacement curve.

Since there is only elastic deformation during unloading, the loading and unloading paths should be different, as shown in the load vs. displacement curve. It can be shown that:

$$S = \frac{dP}{dh} = 2E^* a \tag{3.11}$$

where S is the stiffness of the upper portion of the unloading data. Using the normal definition, hardness is found by:

$$H = \frac{P_{max}}{\pi a^2} \tag{3.12}$$

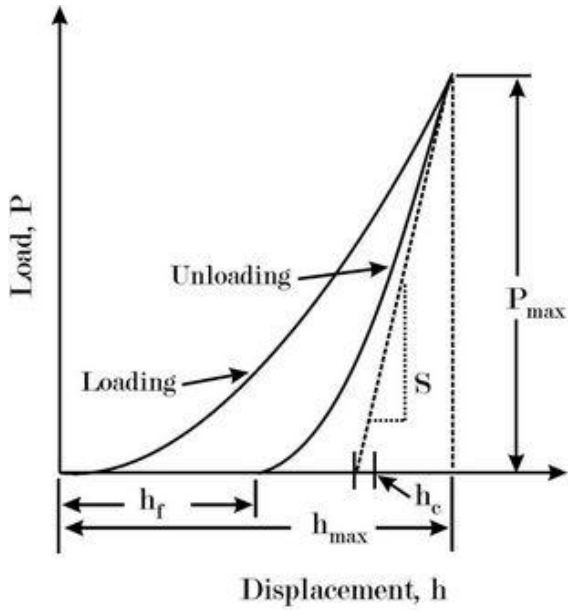

Figure 3-4 Schematic of typical indenter load vs. indenter displacement curve

The main difficulty arises when trying to determine which contact radius a to use. The two obvious choices are contact radius at the maximum indentation depth, h_{max} and contact radius at the final indentation depth h_f. Another possibility which yields better results than that other two is to find a linear fit of the upper portion of the unloading curve, and extrapolate using the contact radius of the intercept. Even this contact radius has significant error as there is rarely any linearity in the unloading curve due to a constant

change in the contact area. The best, and most widely used method, was developed by Oliver and Pharr [12]. It states that during unloading

$$h_p = h_{max} - h_a \tag{3.13}$$

where h_a is the depth at which the contact radius equals that in Equation (3.12) and Equation (3.13). For a conical indenter, it has been shown that

$$h_a = \frac{2}{\pi}(\pi - 2)\frac{P}{S} \tag{3.14}$$

Since the contact radius of interest is at the peak load, Equation (3.14) becomes

$$h_a = \varepsilon \frac{P_{max}}{S} \tag{3.15}$$

where ε is indenter geometry constant. For a conical indenter$\varepsilon = 0.72$, and similar arguments show that $\varepsilon = 1$ for a flat punch and $\varepsilon = 0.75$ for a spherical indenter. The initial unloading stiffness S is found by fitting the unloading curve to a power law of the form

$$p = A\left(h - h_f\right)^m \tag{3.16}$$

with the constants A, h_f, and m found by a least squares fitting procedure. The initial unloading stiffness is then the derivative of Equation (3.16) with respect to h at $h = h_{max}$ equation (3.11) and (3.12), along with the known tip geometry, can now be used to find the elastic modulus and hardness of the specimen.

3.3 Types of Indenter Tip

There are many types of indentation tip, depending on the type of indentation technique. Vickers and knoop are used for microhardness testing and cube-corner, conical, Berkovich, and spherical are used for nanoindentation. Indenter tip can be three sided or four sided pyramid shape. Table 3-1 shows different type of indenter tips and a brief summary of their properties.

Table 3-1Different types of indenter tip and there summary

Vickers Indenter	Cube-Corner Indenter	Berkovich Indenter	Conical Indenter	Sphere Indenter
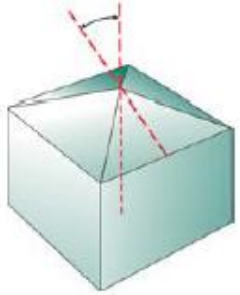	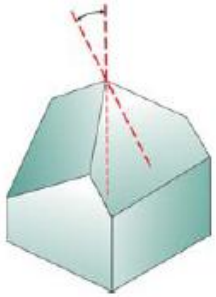	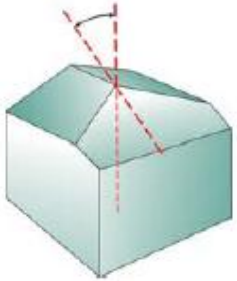	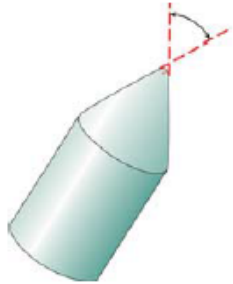	
4 Sided Pyramid	3 sided pyramid with perpendicular faces	3 sided pyramid	Conical	spherical
Centreline to face angle α = 68°	Centreline to face angle α = 35.26°	Centreline to face angle α = 65.3	Angle (Ψ)	-
Area of Projection = $24.50(2a)^2$	Area of Projection = $2.59(2a)^2$	Area of Projection = $24.56(2a)^2$	Area of Projection = πa^2	Area of Projection = πa^2

In the current research work, Vickers indenter tip is used for microhardness testing and cube-corner indenter is used for nanoindentation. These indenters are shown in figure 3-5, imaged under optical microscope and Scanning Electron Microscope (SEM).

The capability of Vickers indenter to produce much larger radial crack without causing chipping in the specimen surface makes itself excel in 1) accuracy of measuring radial cracks, 2) reducing influence of grain size in coarse materials and 3) locate indent efficiently [4].

Cube-corner is a three-sided pyramid type tip which is mainly used due to its ability to exert higher stress at low indentation depth. This is very helpful in thin films and secondly the samples used for our research are DLC thin films which show very high hardness and cannot be cracked by Berkovich tip. It requires very high load to induce sufficient stress to crack the DLC films using Berkovich indenter.

(a) (b)

Figure 3-5 (a) Vickers indenter tip under optical microscope, (b) Cube-corner indenter tip under SEM

3.4 Types of Cracks

When indentation is made at a certain load on brittle materials, it will result in mainly four types of cracks as shown in figure 3-6 a, b, c and d. Cook and Pharr [12] classified this different types of cracks based on their geometry.

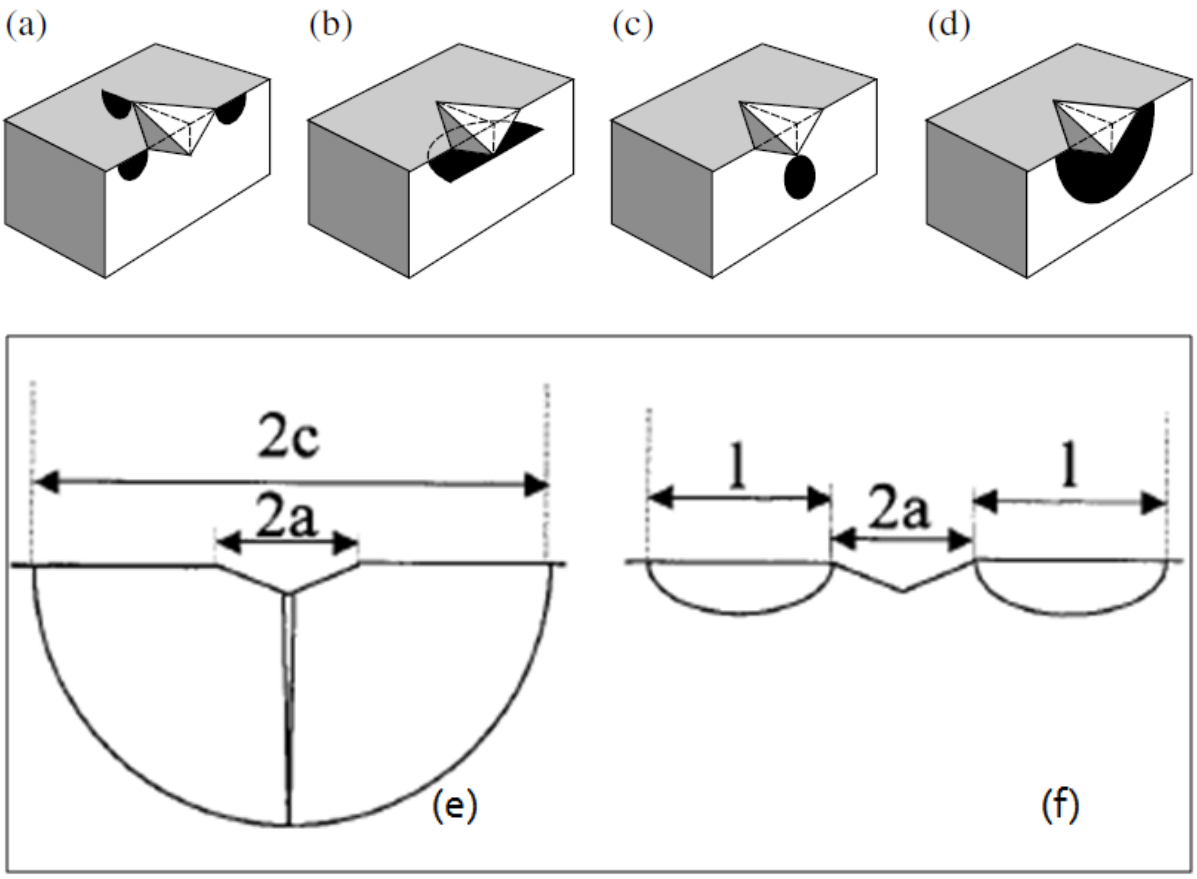

Figure 3-6 (a) Radial/ Palmqvist crack, (b) Lateral crack, (c) Median crack, (d) Half-penny crack (e) Cross-section of Half-Penny Crack and (f) Cross-section of Radial/Palmqvist crack

- If c≥2a, it is half-penny crack pattern (Low toughness) (shown in figure 3-6 e)
- If c<2a, it is Palmqvist/ radial cracking (High toughness) (shown in figure 3-6 f)

It is the radial and half-penny cracks shown in figure 3-6 (e) and (f) of particular importance, since their proximity to the surface has a significant influence on the fracture strength of the specimen. Radial cracks are vertical half-penny type cracks that occur on the surface of the specimen outside the plastic zone and at the corner of the residual impression of indentation. These cracks are generally formed by a hoop stress and extend downwards into the specimen but are usually quiet shallow. Half-penny cracks are formed beneath the surface as median crack and may join upwards with radial surface crack depending on the loading condition; they arise as an action of an outward stress.

3.5 Fracture Toughness

Fracture mechanics treatments of these types of cracks seek to provide a measure of fracture toughness based on the length of the radial surface cracks.

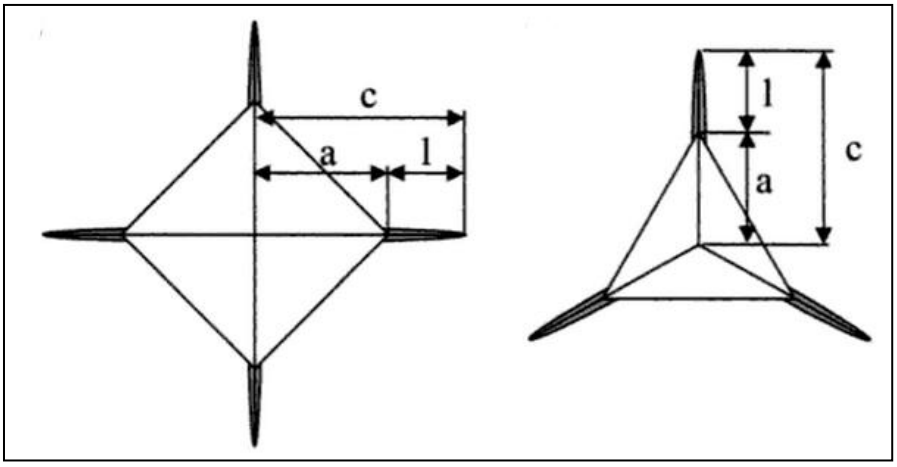

(a) (b)

Figure 3-7 (a) Impression of Vickers indentation and (b) Impression of cube-corner indentation on specimen surface

Crack parameters and indent impression for Vickers and cube-corner tip are shown in figure 3-7 (a) and (b), where crack length c is measured from the center of contact to end of crack at specimen surface.

Palmqvist further proposed that the crack length l varies as a linear function of indentation load. Further Lawn, Evans and Marshall [14] proposed a different relationship and gave a model to characterize fracture toughness.

$$K_{Ic} = k\left(\frac{E}{H}\right)^{n}\frac{P}{c^{3/2}} \tag{3.17}$$

where k is tip empirical constant (0.016 for Vickers and 0.032 for Cube corner), n=1/2, E is modulus of elasticity (GPa), H is hardness (GPa), P is Load (N) and c is crack length. This was the first fracture toughness model, and it was further modified by many people [12-14, 18, 20, 22-30]

3.6 Fracture in Thin Films

Fracture process in thin films can be very complicated. It is proposed that fracture toughness in thin film occurs in three stages as shown in figure 3-8. (1) First ring-like through-thickness cracks form around the indenter by high stresses in the contact area, (2) Delamination and buckling occur around contact area at the film substrate interface by high lateral pressure, (3) Second ring-like through-thickness cracks and spalling are generated by high bending stresses at the edges of the buckled film.

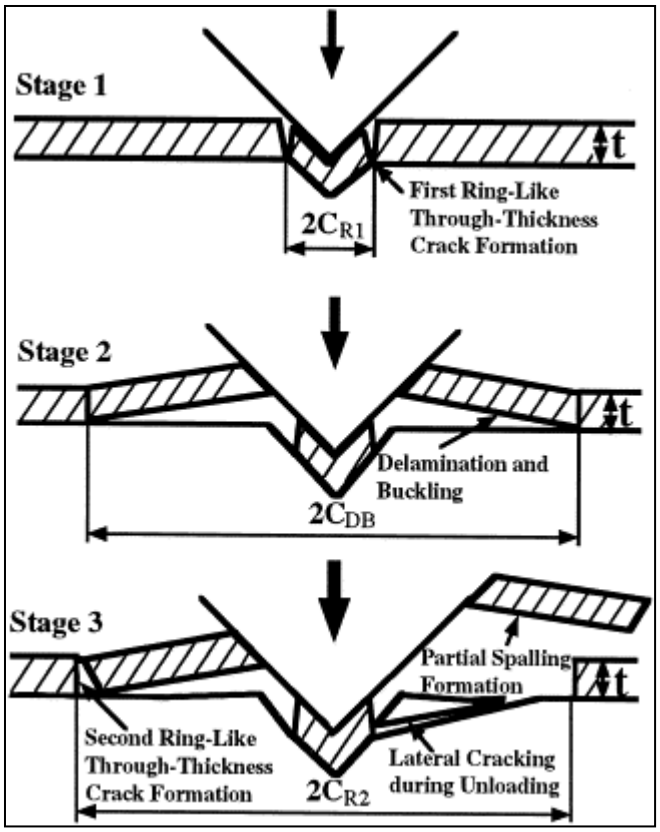

Figure 3-8 Schematic of various stages of indentation fracture in film/substrate system

In the first stage, if the film under the indenter is separated from the bulk film via the first ring-like through-thickness cracking, a corresponding step will be present in the loading curve. If discontinuous crack form's and the film under the indenter is not separated from the remaining film, no step appears in the loading curve because the film still supports the indenter and the indenter cannot suddenly advance into the material. In the second stage, buckling are not big enough to form steps in the loading curve because the film around the indenter still supports the indenter, but generate discontinuities which change the slope of the loading curve with increasing indentation loads. In the third stage, the stress concentration at the end of the interfacial crack cannot be relaxed by the propagation of the interfacial crack. With an increase in indentation depth, the height of

the bulged film increases. When the height reaches a critical value, the bending stress caused by the bulged film around the indenter will result in the second ring-like through-thickness crack formation and spalling at the edge of the buckled film, as shown in figure 3-8 stage three. This leads to a step in the loading curve. This is a single event and results in the separation of the part of the film around the indenter from the bulk film via cracking through films. The step in the loading curve is entirely from the film cracking and not from the interfacial cracking or the substrate cracking.

3.7 Fracture Toughness Models

First fracture toughness model was proposed by Lawn and Evans [14] and modified by various people to find the most optimum model. They are classified mainly based on the crack geometry and size.

3.7.1 For Vickers Indentation with Half-penny Crack

(1) Evans et al. [13] & Lawn et al. [14] developed an equation which allows the determination of K_{Ic} from indentation experiments by measuring the length of cracks emanating from the edges of the indent impression [3]:

(H1) $$K_{Ic} = 0.014\left(\frac{E}{H}\right)^{\frac{1}{2}}\left(\frac{P}{c^{1.5}}\right) \tag{3.18}$$

(2) Lawn and Fuller [20] together, based on dimensional consideration deduced that ratio $\left(\frac{P}{C^{1.5}}\right)$ should be constant and gave equation:

(H2) $$K_{Ic} = 0.0726\left(\frac{P}{c^{1.5}}\right) \tag{3.19}$$

(3) Based on Lawn and Fuller [20] equation Evan & Charles [18] derived a widely applicable but still semi-empirical formula for the toughness on the basis of dimensional analysis and empirical curve fitting:

(H3) $$K_{Ic} = 0.16Ha^{1/2}\left(\frac{c}{a}\right)^{-1.5} \tag{3.20}$$

where a is length of indent diagonal from the center of indentation

(4) Lawn et al [14,20] , who explicitly resolved the complex elastic-plastic stress field beneath the indentation into a reversible elastic stress field component and an irreversible residual stress field component, derived the following equation based on Evans and Marshall's [21] work:

(H4) $K_{Ic} = 0.028H(a)^{\frac{1}{2}}\left(\frac{E}{H}\right)^{\frac{1}{2}}\left(\frac{a}{c}\right)^{1.5}$ (3.21)

(5) Based on Lawn et al [14, 20], Antis & Chatikul [22], by empirical fitting of fracture toughness data of a variety of ceramics they calibrated the scaling factor and obtained:

(H5) $K_{Ic} = 0.016\left(\frac{E}{H}\right)^{\frac{1}{2}}\left(\frac{P}{c^{1.5}}\right)$ (3.22)

(6) Antis et al [22] also derived two separate equations for fracture toughness in brittle materials:

(H6) $K_{Ic} = 0.8193 \times H^{0.5} \times E^{0.5} \times a^2 \times c^{-1.5}$ (3.23)

(H7) $K_{Ic} = 1.3627 \times H^{0.5} \times E^{0.5} \times a^2 \times c^{-1.5}$ (3.24)

(7) Niihara and co-workers [23, 24] modified Evans and Lawn [13, 14] equation by introducing a different exponent of (E/H), namely 2/5 instead of 1/2. They gave following expressions for fracture toughness, for halfpenny cracks with c/a ≥ 2.5:

(H8) $K_{Ic} = 2.1097 \times H^{0.6} \times E^{0.4} \times a^2 \times c^{-1.5}$ (3.25)

(H9) $K_{Ic} = 0.033\left(\frac{E}{H}\right)^{\frac{2}{5}}\left(\frac{P}{c^{-1.5}}\right)$ (3.26)

(8) Laugier [25] used an analytical approximation of the relative plastic zone size for input into Hill's expanding cavity model and obtained a non-dimensional factor $(\frac{E}{H})^{2/3}$

instead of $(\frac{E}{H})^{1/2}$, which was introduced by Lawn et al. [13,14]. Laugier [25] showed that $(\frac{E}{H})^{2/3}$ gave the better fitting to experimental data. His formula has the form:

(H10) $K_{Ic} = 1.073 \times 0.015 \times \left(\frac{a}{l}\right)^{\frac{1}{2}} \times (E/H)^{2/3} \times \left(\frac{P}{c^{1.5}}\right)$ (3.27)

l is crack length from the edge of indentation

3.7.2 For Vickers Indentation with Palmqvist Crack

(1) Lawn & Fuller [20] derived:

(P1) $K_{Ic} = 0.0515\left(\frac{P}{c^{3/2}}\right)$ (3.28)

(2) Evans & Wilshaw [27] derived:

(P2) $K_{Ic} = 0.079\left(\frac{P}{a^{3/2}}\right)\log\left(4.5\frac{a}{c}\right)$ (3.29)

(3) Niihara & co-workers [23, 24] also derived equation for Palmqvist crack with a low crack-to-indent size ratio 0.25 ≤ l/a ≤ 2.5:

(P3) $K_{Ic} = 0.009 \times \left(\frac{E}{H}\right)^{\frac{2}{5}} \times \left(\frac{P}{a\sqrt{l}}\right)$ (3.30)

(4) Shetty et al. [28] used a wedge-loaded crack as a fracture mechanical analogue to the situation in Palmqvist cracks. They derived an equation without any further empirical fitting:

(P4) $K_{Ic} = 6.6637Hal^{-0.5}$ (3.31)

3.7.3 For Cube-corner Indentation

(1) Evans et al. [13] & Lawn et al. [14] developed an equation which allows the determination of K_{Ic} from indentation experiments by measuring the length of cracks emanating from the edges of the indent impression [29]:

(C1) $K_{Ic} = 0.032 \times \left(\frac{E}{H}\right)^{\frac{1}{2}} \times \left(\frac{P}{c^{1.5}}\right)$ (3.32)

(2) Jang & Pharr [30] developed an analytical expression which correlates tip empirical constant with indenter opening angle:

$$\text{(C2)} \quad K_{Ic} = \frac{0.0443}{1-v} \times \left(\frac{E}{H}\right)^{\frac{1}{2}} \times \left(\frac{P}{c^{1.5}}\right) \tag{3.33}$$

(3) Laugier[25] used an analytical approximation of the relative plastic zone size for input into Hill's expanding cavity model and obtained a non-dimensional factor $(\frac{E}{H})^{2/3}$ instead of $(\frac{E}{H})^{1/2}$, which was introduced by Lawn et al. [13,14]. Laugier showed that $(\frac{E}{H})^{2/3}$ gave the better fitting to experimental data. His formula has the form:

$$\text{(C3)} \quad K_{Ic} = 0.015 \times (a/l)^{1/2} \times (E/H)^{2/3} \times \left(\frac{P}{c^{1.5}}\right) \tag{3.34}$$

(4) Work approach method to determine fracture toughness, in this model the Lawn et al. [14] model is modified. It was found that ratio of hardness to elastic modulus is sensitive to radial crack, whereas the ratio of unloading work (W_u) to total loading work (W_t) is not. Based on this finding a new equation was proposed.

$$\frac{E}{H} = \frac{1}{1.07k} \times \frac{Wt}{Wu}$$

Substituting above equation in Lawn equation we get:

$$\text{(C4)} \quad K_{Ic} = \lambda \times \left(\frac{Wt}{Wu}\right)^{\frac{1}{2}} \times \left(\frac{P}{c^{1.5}}\right) \tag{3.35}$$

where $\lambda = \frac{\delta}{\sqrt{1.07k}}$, δ is the indenter tip empirical constant, using the load vs. displacement curve from figure 3-9, one can measure the work done during loading of indenter and unloading the indenter. Using a standard sample, new tip empirical constant is measured (λ). This eliminates the error found in (E/H). This method uses a standard reference to measure the error factor and set calibration to make the result accurate.

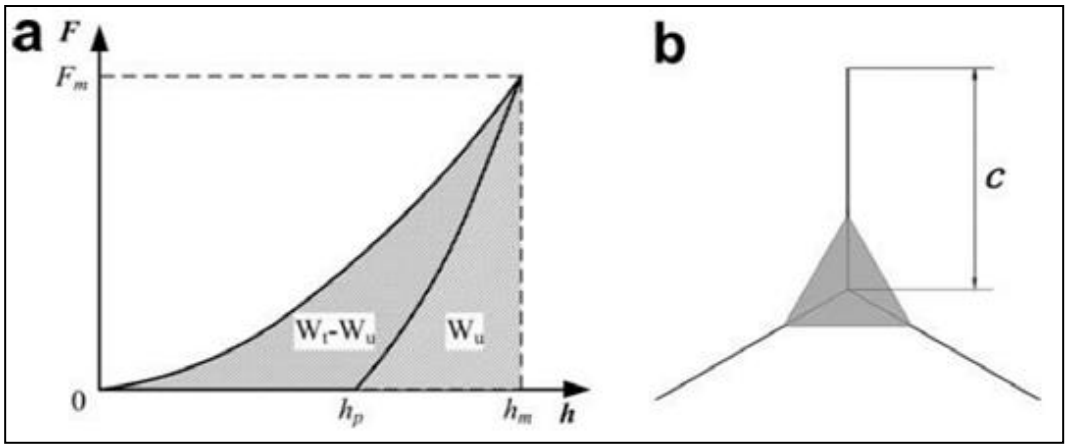

Figure 3-6

Figure 3-9 (a) Peak load (F_m), unloading work (W_u) and total loading work (W_t), (b) length of radial crack c

5) Fracture toughness characterization by strain energy released during cracking. In this method circumferential cracking and spallation are checked to observe peeling of the coatings around indentation, for brittle coatings it is observed in nanoindentation. During cracking and spallation, a plateau forms in load-displacement curve as shown in figure 3-10. This step/plateau represents the associated energy released during the cracking of thin films.

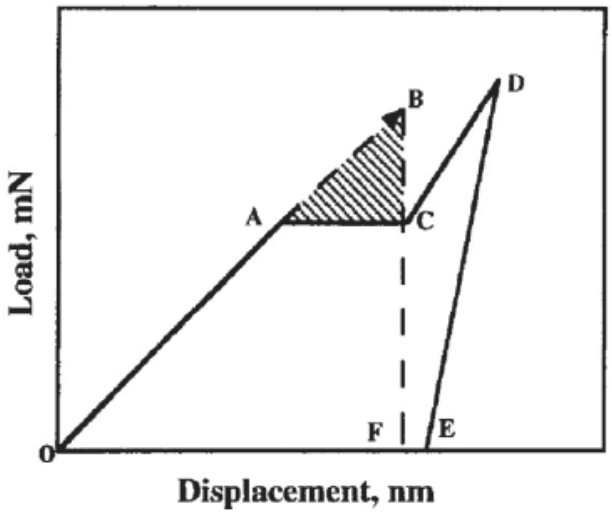

Figure 3-10 Schematic of load-displacement curve, showing a step/plateau during loading cycle

From previous study of thin films fracture we know fracture proceeds as follows: (1) the first circumferential through-thickness crack forms around the indenter by high stress in the contact area (2) delamination and buckling occur around the contact area at the coating/substrate interface due to high lateral pressure (3) a second circumferential through-thickness crack forms, and spallation is generated by high bending stresses at the edges of the buckled thin coating. The stage of circumferential through-thickness cracking of the coating causes a sudden excursion of the indenter in displacement, which induces a step in the load–displacement curve. Figure 3-10 given area ABC representing the energy U dissipated upon coating cracking, the fracture toughness is obtained as:

$$\text{(C5)} \quad K_{Ic} = \left[\left(\frac{E}{(1-\nu^2)2\pi c}\right)\left(\frac{U}{t}\right)\right]^{\frac{1}{2}} \tag{3.36}$$

where ν is Poisson's ration and t is thin film thickness.

Chapter 4

Experimental Procedure

Initially standard samples are analysed under microhardness testing and nanoindenter to check the calibration of the machine. Standard steel block of LECO was used for microhardness testing and Fused Quartz sample was used for Nanoindenter.

(100) Single crystal Si wafer were used for fracture toughness analysis in brittle substrate material and the same type of Si wafer were coated with 0.4 µm (400 nm) & 0.85 µm (850 nm) thick DLC thin films using Magnetron Sputtering. Sample surface was clean and flat and did not require any polishing or surface finishing. X-ray Diffraction (XRD) analysis was conducted to make sure the Si was (100). Using profilometer coating thickness of DLC where measured.

Indentations were carried out on all 3 samples using microhardness testing starting from 25 gf load, 5 sets of indentation where carried out. Load was increased up to 500 gf and the indentations were stopped at load where sample started to buckle or thin films resulted in spalling or secondary crack propagation. Using the attached microscope with measuring scale in the microhardness testing indentation diagonal a and indentation crack lengths c are measured. All the indentations were made by Vickers indenter tip only.

Another set of indentations were carried out to measure fracture toughness using nanoindenter, using the cube-corner tip. Different loads were selected from a range of 1000 to 10000 µN. Si showed cracks in all load range, however cracking DLC thin films was very hard. Indentations imaging was carried out using the AFM, equipped in nanoindentation testing. Surface topography was generated after each indentation. Using the scan area size scale, crack length was measured in the indentation image. Using all

the indentation parameters and results, different fracture toughness models were applied based on crack and indentation geometry.

Chapter 5

Results and Discussion

5.1 Calibration Sample Analysis

Two Instruments are used for indentation, microhardness testing and nanoindentation testing and there calibration results are discussed.

5.1.1 Calibration Check for Microhardness Testing

Standard Steel Block of LECO having hardness of 776 HV, Calibrated at 500 gf was used for checking the calibration of microhardness testing. The result is discussed in table 5-1 and figure 5-1.

Table 5-1 Microhardness testing result for standard steel block of 776 HV hardness

Load (gf)	Hardness (HV)
1000	763.28
500	760.15
300	753.70
200	741.48
100	728.15
50	674.80
25	637.41
10	520.48

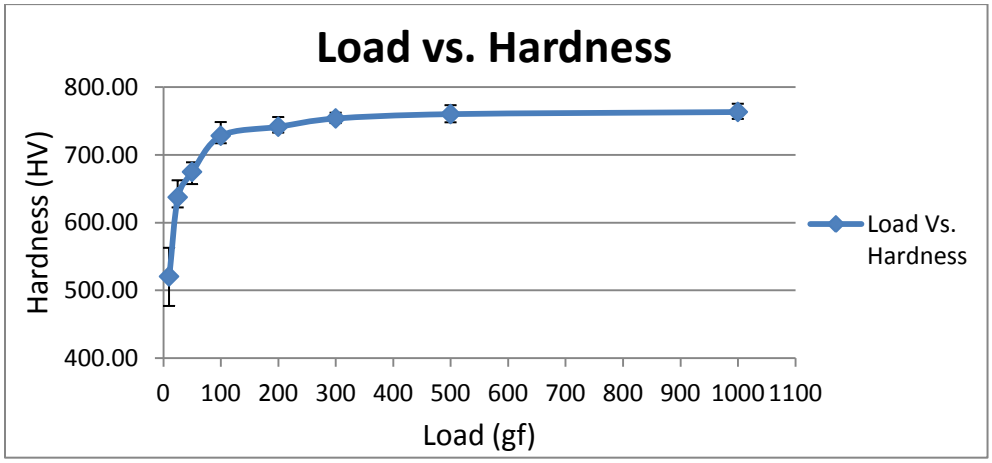

Figure 5-1 Load vs. Hardness curve for standard steel sample

Standard steel sample with hardness of 776 HV was used. microhardness testing is showing good agreement in result for load in range 100 to 1000 gf. However it is showing a decrease in hardness value for load 10, 25 and 50 gf. The error is very high for the 10 gf load. This is due to the fact that diagonal length values are in the range of micrometers and the precision of reading using optical microscopy is ± 0.5 μm in length. Thus, at low loads small measurement errors will produce large hardness deviations [15].

5.1.2 Calibration Check for Nanoindentation Testing.

Fused Quartz with standard hardness of 9.25 GPa and Modulus of 72 GPa is used for calibration of nanoindentation. Three indentations are made and the result is in good agreement with standard result. It can be seen in figure 5-2, nanoindentation analysis made on the fused Quartz sample using cube-corner indenter at 5000 μN load.

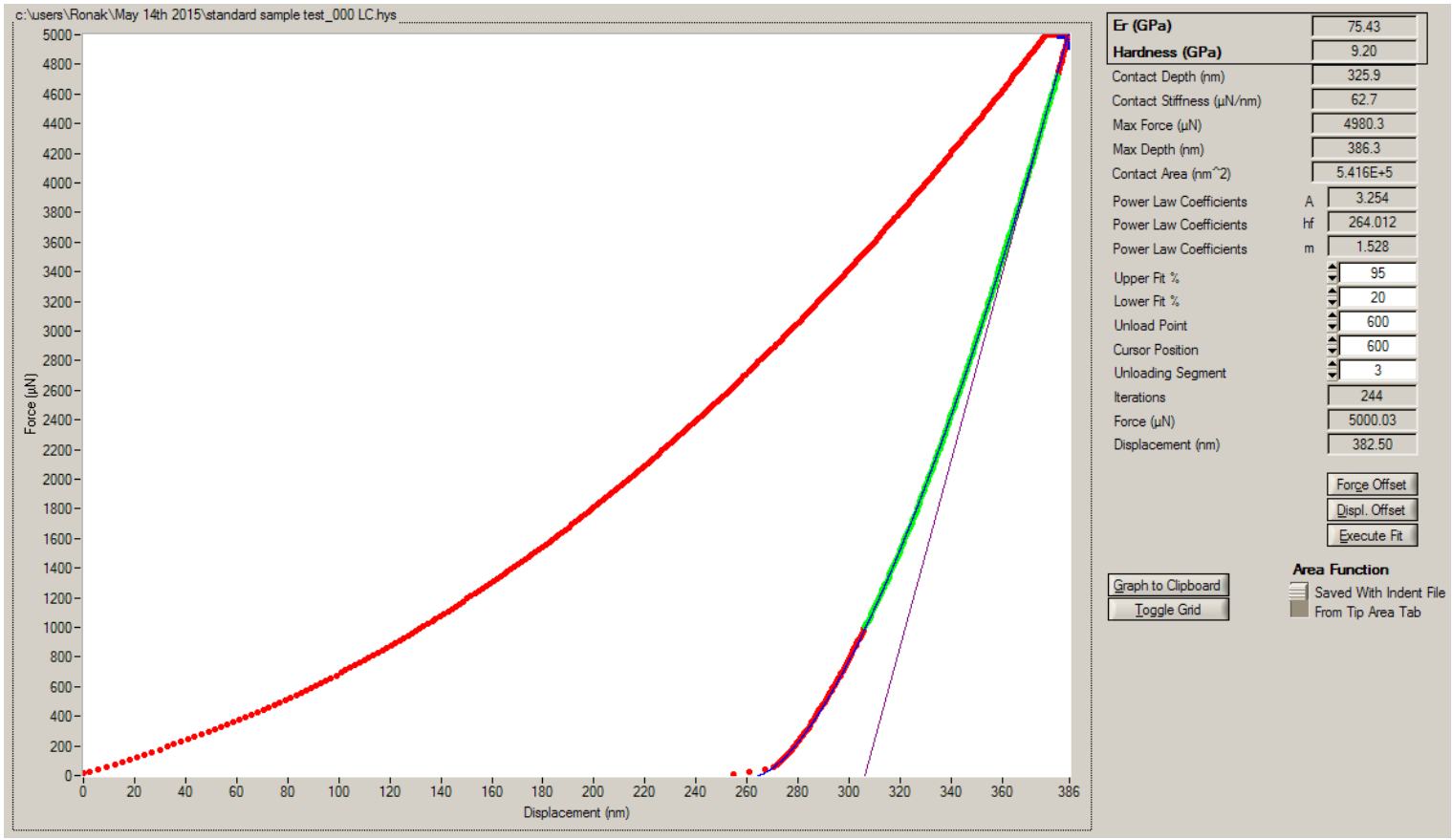

Figure 5-2 Nanoindentation analysis of standard fused Quartz sample

5.2 DLC Coating Thickness Measurement using Profilometer

After coating Si with DLC thin film, coating thickness can be measured using white light profilometer. Two DLC thin films coated by Magnetron Sputter are analyzed under profilometer to measure the coating thickness. Results analyzed are discussed in figures 5-3 and 5-4, showing coating thickness of 0.4 and 0.85 μm of DLC.

5.2.1 Profilometer analysis of 0.4 μm DLC

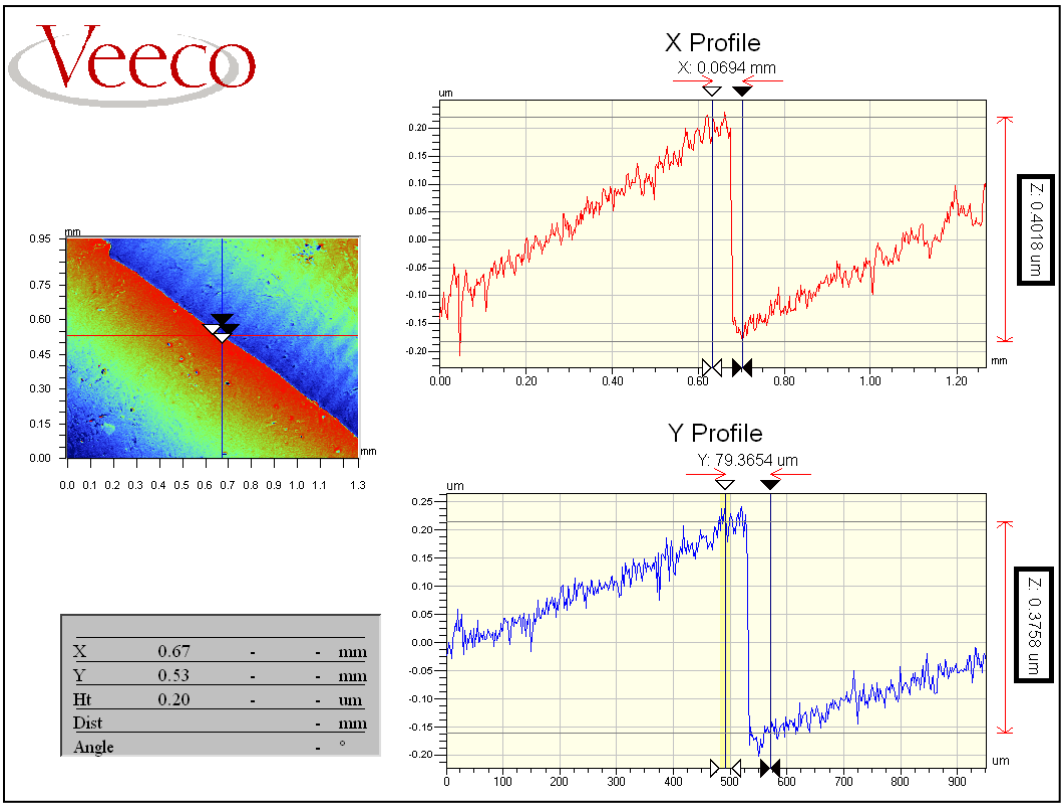

Figure 5-3 Coating thickness measurement using Profilometer for 0.4μm DLC thin film

5.2.2 Profilometer analysis of 0.85 μm DLC

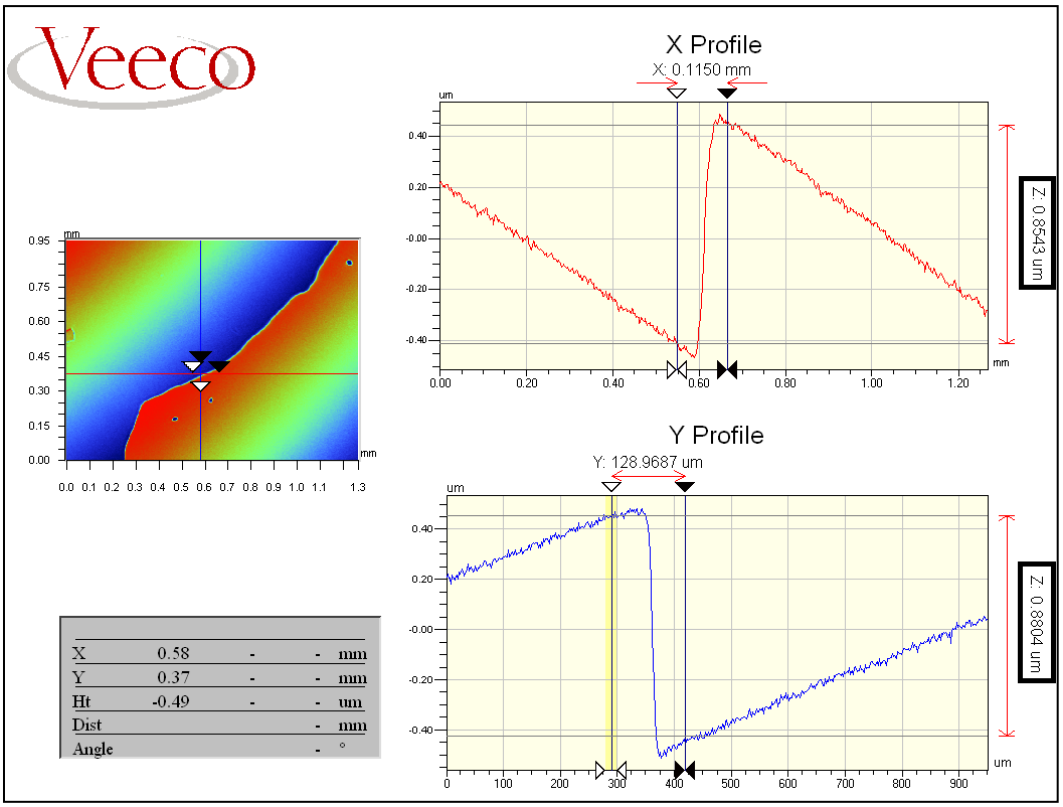

Figure 5-4 Coating thickness measurement using Profilometer for 0.85μm DLC thin film

5.3 Fracture Toughness Measurement of (100) Single Crystal Si using Vickers Indenter

Si wafer with thickness of 0.34 mm is indented using microhardenss testing to measure fracture toughness. Size of indent diagonal and crack length are measured using microscopic scale attached to microhardness testing machine. Different fracture toughness model for Vickers indenter are applied to measure fracture toughness of (100) single crystal Si. All the results for different models at different load are presented in table 5-2. Figure 5-5 shows comparison of different fracture toughness models measured at different loads. Figure 5-6 shows load vs. hardness for Si measured in a microhardness testing. The indentation images on Si surface are shown in figure 5-7.

Table 5-2 Fracture toughness measurement using half-penny crack models for (100) single crystal Si using Vickers indenter

Si wafer	
Thickness	0.34 mm
Modulus of Elasticity	145.96 GPa
Lit Hardness	8.7 GPa
Literature K_{Ic}	0.95 $MPa\sqrt{m}$

		Lawn and Evans	Lawn and Fuller	Evans and Charles	Lawn based on Evans and Marshall
Load (gf)	Hardness (GPa)	H1 K_{Ic} $MPa\sqrt{m}$	H2 K_{Ic} $MPa\sqrt{m}$	H3 K_{Ic} $MPa\sqrt{m}$	H4 K_{Ic} $MPa\sqrt{m}$
100	8.57	0.67	0.84	0.86	0.62
50	8.69	0.76	0.97	0.99	0.71
25	7.22	0.74	0.85	0.87	0.68

	Antis and Chatikul	Antis et al. (1)	Antis et al. (2)	Niihara et al. (1)	Niihara et al. (2)	Laugier
Load (gf)	H5 K_{Ic} $MPa\sqrt{m}$	H6 K_{Ic} $MPa\sqrt{m}$	H7 K_{Ic} $MPa\sqrt{m}$	H8 K_{Ic} $MPa\sqrt{m}$	H9 K_{Ic} $MPa\sqrt{m}$	H10 K_{Ic} $MPa\sqrt{m}$
100	0.77	0.57	0.96	1.11	1.19	0.97
50	0.87	0.65	1.09	1.27	1.36	1.31
25	0.84	0.63	1.05	1.21	1.29	1.48

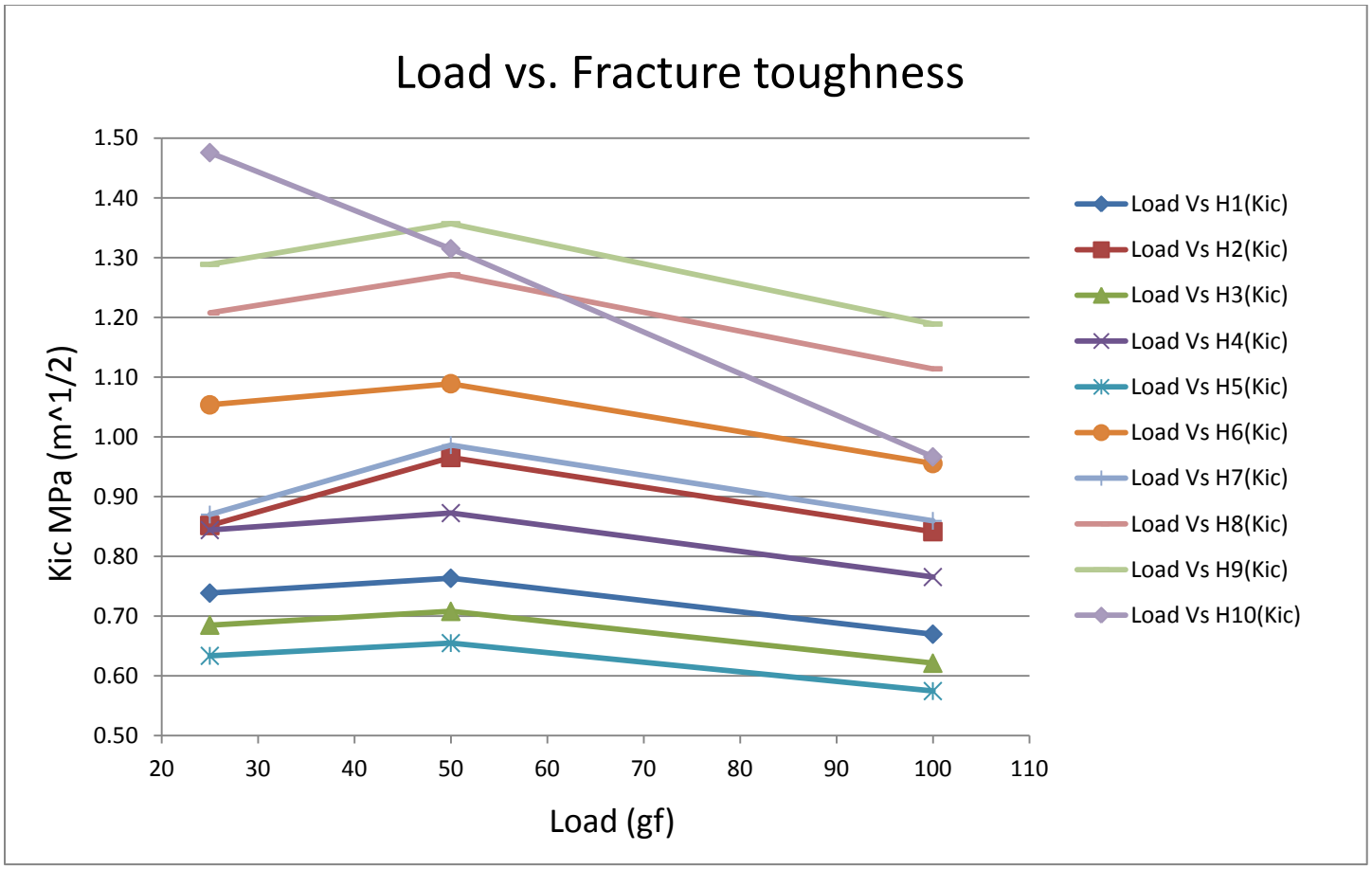

Figure 5-5 Graph of load vs. fracture toughness for different half-penny crack models, measured on single crystal Si

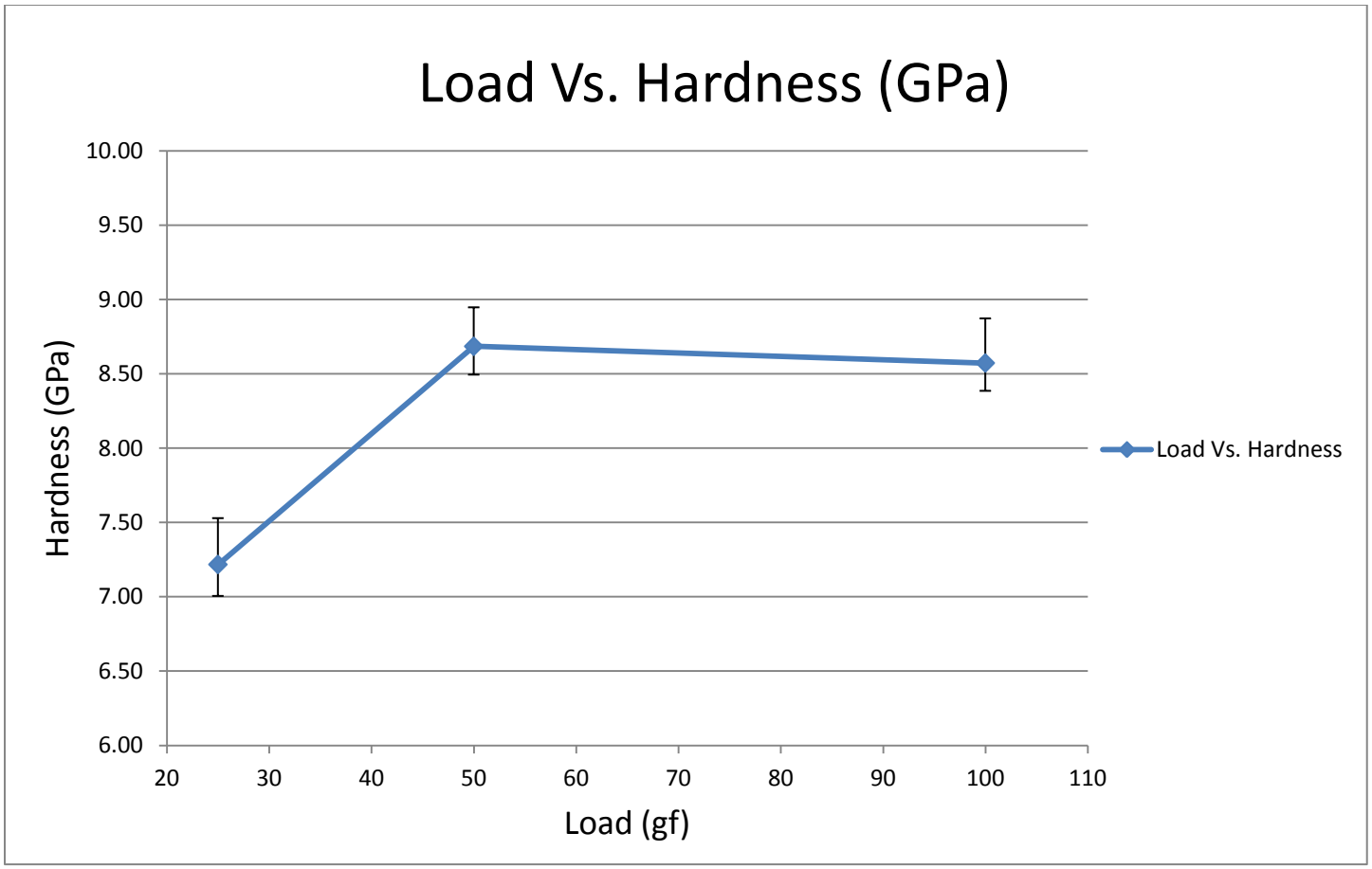

Figure 5-6 Graphs of load vs. hardness for single crystal Si

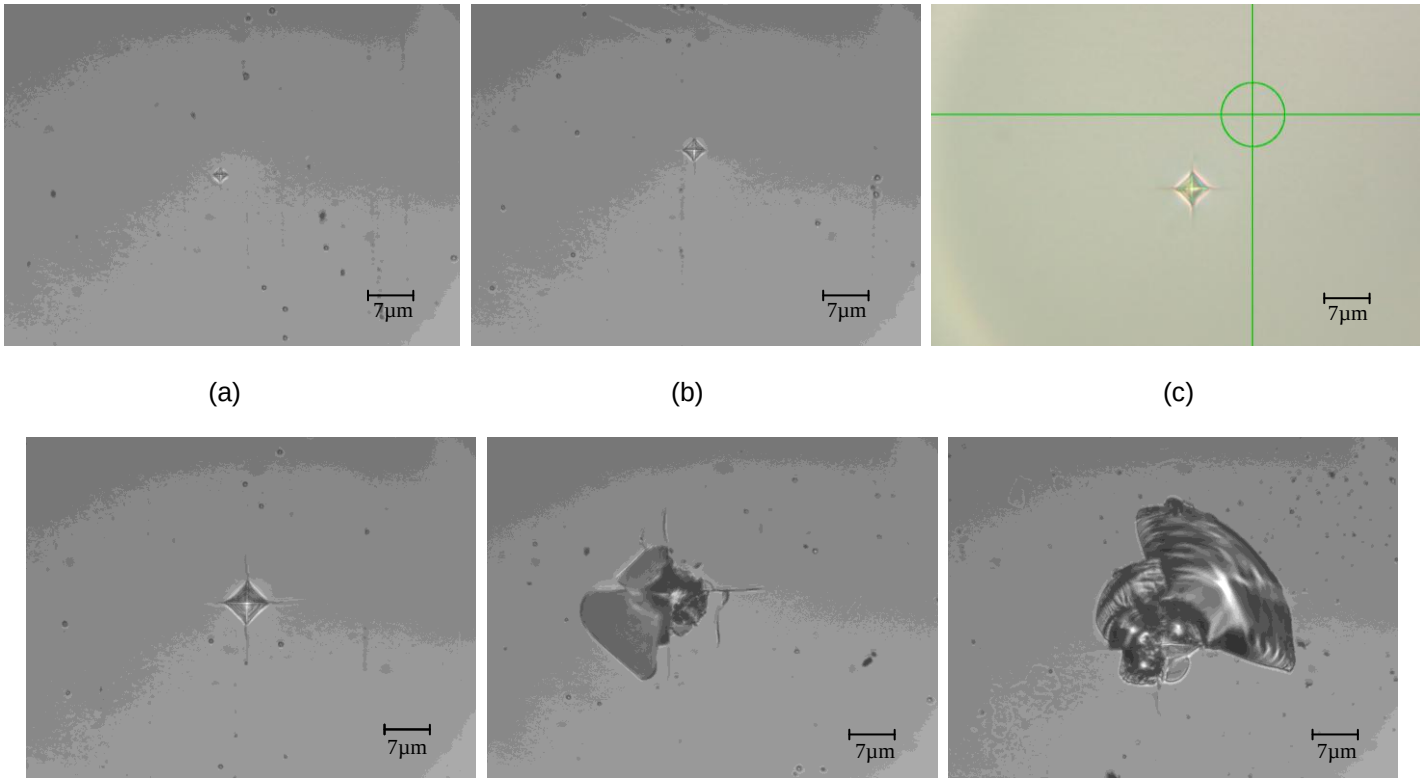

Figure 5-7 Vickers indentation image at 500X magnification on Si surface, at load (a) 10 gf, (b) 25 gf, (c) 50 gf, (d) 100 gf, (e) 200 gf and (f) 200 gf

(100) single crystal Si wafer has a standard hardness of 8.7 GPa. It was indented by Vickers indenter using a microhardness testing machine. Indenter was aligned in the direction of cleavage plane of Si wafer. Multiple indentations are made on Si at load of 25, 50 and 100 gf and are imaged for study of fracture toughness. Additionally Si was indented using nanoindenter to measure the modulus of elasticity. Average modulus of 10 indentations readings was 145.96 GPa.

All microhardness indentation showed half-penny type cracks (c > 2a). All fracture toughness measuring model from H1 to H10 are applied to measure the fracture toughness and all the models showed slight variation in the results. Standard fracture toughness (K_{Ic}) measured for Si is 0.95 $MPa\sqrt{m}$. H2 (Lawn and Fuller), H4 (Lawn based on Evans and Marshall), H7 (Antis et al. (equation 2)) models showed the best results for the fracture toughness measurement.

Lawn and Fuller equation is based on dimensional consideration and the hardness of the material depends only on the crack length. Lawn based on Evans and Marshall derived his model by considering the crack length and hardness but he also considered the diagonal length of indenter to measure fracture toughness. Antis et al. derived two equations for fracture toughness model with different tip empirical constants, where the second equation fits the best with tip empirical constant of 1.362. Tip empirical constant plays a very important role for any given material. Different materials behave differently for given indenter tip.

All the other plots show slight variation due to different approach in the tip empirical constant in the fracture toughness models with respect to other constraints of material such as hardness, crack length and diagonal of indent. However these models do not give very good result due the error, mainly in the tip empirical constant.

In the figure 5-6 load vs. hardness curve, it is observed that at low load the hardness drops significantly. However, figure 5-5 shows that fracture toughness is not decreasing much with decrease in load.

Indent at 10 gf load shown in figure 5-7 (a) yield no radial cracks. All the indent images (b), (c) and (d) in Figure 5-7 show very clean radial crack from the top view whereas at higher load of 200 gf, they show secondary cracks and buckling of Si. These indentations are not considered as they yield high error in results.

5.4 Fracture Toughness Measurement of 0.4 μm DLC using Vickers Indenter

0.4 μm DLC thin film coated on Si substrate is indented by Vickers indenter using a microhardness testing machine. Size of indent diagonal and crack length are measured using microscopic scale attached to microhardness testing machine. Different fracture toughness model for Vickers indenter are applied to measure fracture toughness of 0.4 μm DLC. All the results for different models at different load are presented in table 5-3. Figure 5-8 shows comparison of different fracture toughness models measured at different loads. Figure 5-9 shows load vs. hardness for 0.4 μm DLC measured in a microhardness testing. The indentation images on specimen surface are shown in figure 5-10.

Table 5-3 Fracture toughness measurement using half-penny crack models for 0.4 µm DLC using Vickers indenter

0.4 µm DLC on Si	
Hardness	18.345 GPa
Modulus of Elasticity	115.6 GPa

	Lawn and Evans	Lawn and Fuller	Evans and Charles	Lawn based on Evans and Marshall	Antis and Chatikul
Load (gf)	H1 K_{Ic} $MPa\sqrt{m}$	H2 K_{Ic} $MPa\sqrt{m}$	H3 K_{Ic} $MPa\sqrt{m}$	H4 K_{Ic} $MPa\sqrt{m}$	H5 K_{Ic} $MPa\sqrt{m}$
500	0.42	0.86	1.91	0.84	0.48
300	0.46	0.95	2	0.88	0.53
200	0.48	1	2.15	0.94	0.55
100	0.58	1.19	2.56	1.13	0.66
50	0.58	1.21	2.7	1.19	0.67

	Antis et al. (1)	Antis et al. (2)	Niihara et al. (1)	Niihara et al. (2)	Laugier
Load (gf)	H6 K_{Ic} $MPa\sqrt{m}$	H7 K_{Ic} $MPa\sqrt{m}$	H8 K_{Ic} $MPa\sqrt{m}$	H9 K_{Ic} $MPa\sqrt{m}$	H10 K_{Ic} $MPa\sqrt{m}$
500	0.78	1.29	1.67	0.82	0.42
300	0.81	1.35	1.74	0.9	0.51
200	0.87	1.45	1.87	0.95	0.59
100	1.04	1.73	2.23	1.13	0.86
50	1.1	1.82	2.35	1.14	1

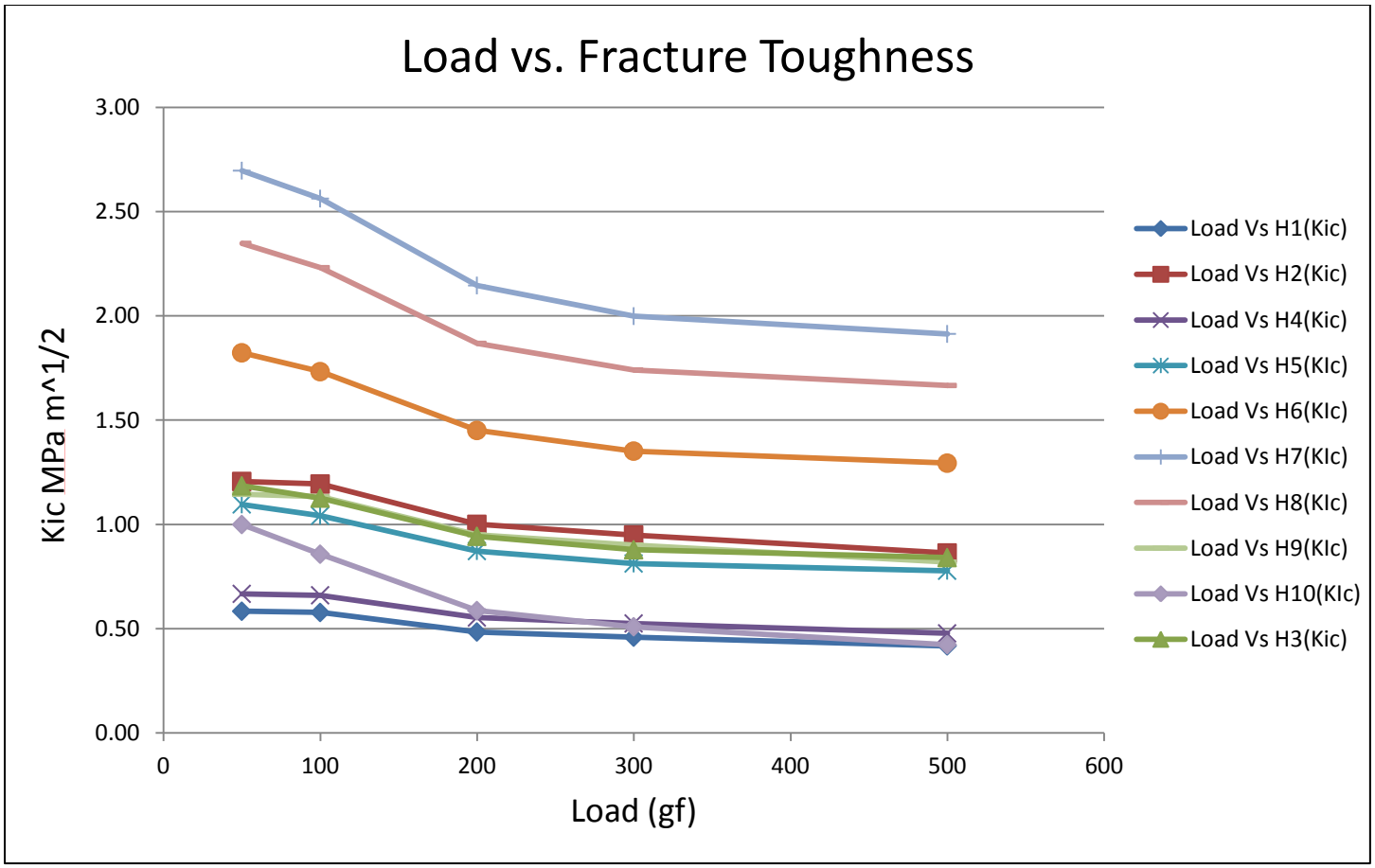

Figure 5-8 Graph of load vs. fracture toughness for different half-penny crack models, measured on 0.4 μm DLC thin film

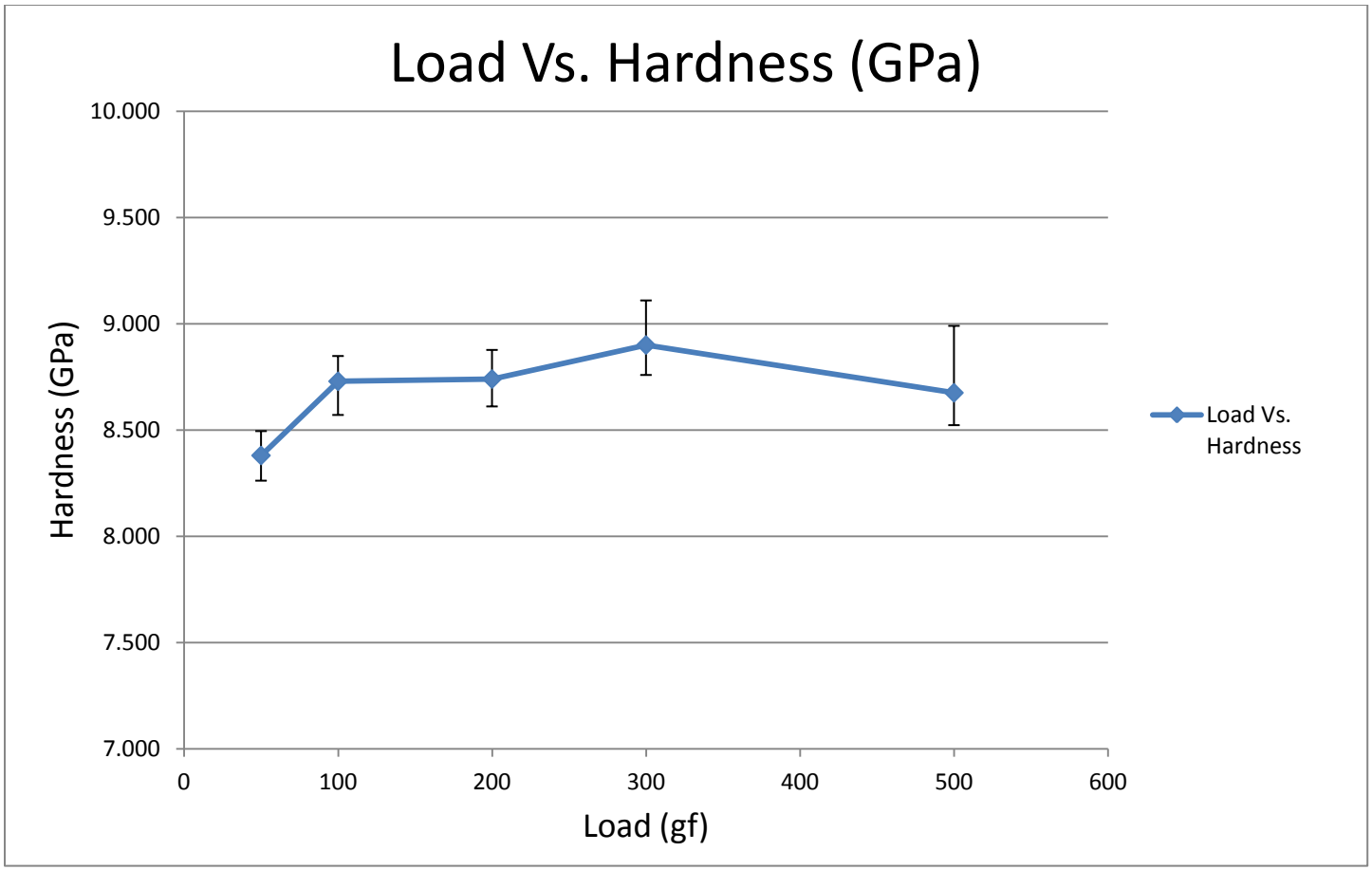

Figure 5-9 Graphs of load vs. hardness for 0.4 µm DLC thin film

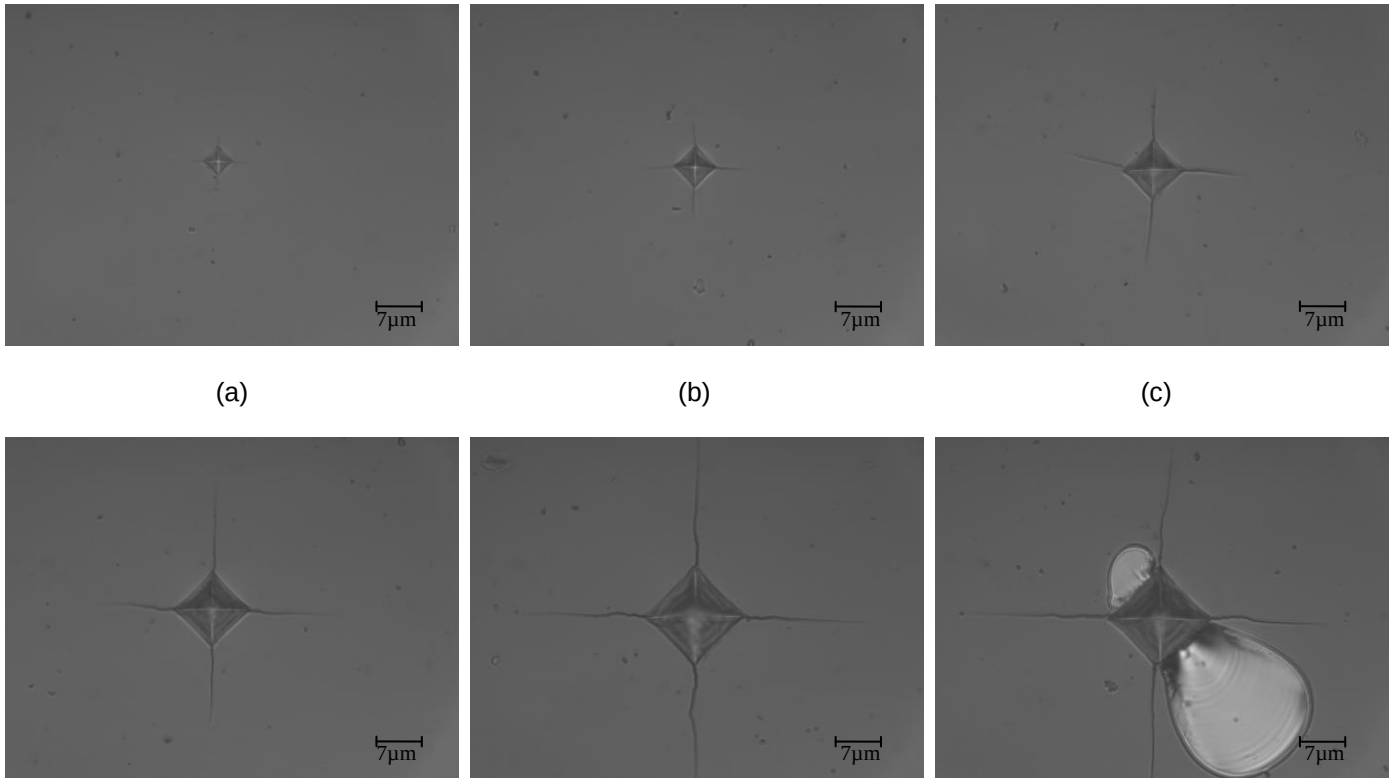

Figure 5-10 Vickers indentation image at 500x magnification on 0.4 μm DLC thin film surface, at load (a) 50 gf, (b) 100 gf, (c) 200 gf, (d) 300 gf, (e) 500 gf and (f) 500 gf

Indenting using Vickers indenter exceeded 10% of DLC coating thickness and the hardness result was incorrect. To eliminate effect of Si substrate 0.4 µm DLC was indented in nanoindenter for measuring the hardness and modulus of elasticity. Indentation made using nanoindenter was made below 10% thickness of 0.4 µm DLC coating and the result was 18.34 GPa hardness and 115.6 GPa modulus of elasticity.

DLC thin film was indented by Vickers indenter tip using a microhardness testing at load 500, 300, 200, 100 and 50 gf. All the cracks are half-penny type crack and accordingly H1 to H10 models are used to measure fracture toughness.

None of the fracture toughness measured are correct. All the measurements are showing fracture toughness similar to the Si fracture toughness results. Due to high indentation load, indenter is penetrating to the Si substrate and the resulting in fracture toughness measurement error. Lower loads are giving higher fracture toughness value due to less penetration in substrate layer.

Antis et al. (equation 2) and Niihara et al. (equation 1) models are giving highest result and both are taking the indentation diagonal in to consideration for their models, giving result a bit closer to the actual fracture toughness.

The load vs. hardness curve in figure 5-9 shows same pattern as observed in the single crystal Si, hardness decreasing at lower load and then it is almost constant. Indentation image captured in figure 5-10 show clean radial crack initiate at load 50 gf. Buckling of DLC film is observed at 500 gf load in figure 5-10 (f), this indentation is not considered because it gives error in result.

5.5 Fracture Toughness Measurement of 0.85 μm DLC using Vickers Indenter

0.85 μm DLC thin film coated on Si substrate is indented by Vickers indenter using a microhardness testing machine. Size of indent diagonal and crack length are measured using microscopic scale attached to microhardness testing machine. Different fracture toughness model for Vickers indenter are applied to measure fracture toughness of 0.85 μm DLC. All the results for different models at different load are presented in table 5-4. Figure 5-11 shows comparison of different fracture toughness models measured at different loads. Figure 5-12 shows load vs. hardness for 0.85 μm DLC measured in a microhardness testing. The indentation images on specimen surface are shown in figure 5-13.

Table 5-4 Fracture toughness measurement using half-penny crack models for 0.85 µm DLC using Vickers indenter

0.85 µm DLC on Si	
Hardness	17.89 GPa
Modulus of Elasticity	107.48 GPa

	Lawn and Evans	Lawn and Fuller	Evans and Charles	Lawn based on Evans and Marshall	Antis and Chatikul
Load (gf)	H1 K_{Ic} $MPa\sqrt{m}$	H2 K_{Ic} $MPa\sqrt{m}$	H3 K_{Ic} $MPa\sqrt{m}$	H4 K_{Ic} $MPa\sqrt{m}$	H5 K_{Ic} $MPa\sqrt{m}$
500	0.57	1.21	2.44	1.05	0.65
300	0.63	1.33	2.6	1.12	0.72
200	0.71	1.51	3.04	1.3	0.81
100	0.9	1.91	3.95	1.7	1.03

	Antis et al. (1)	Antis et al. (2)	Niihara et al. (1)	Niihara et al. (2)	Laugier
Load (gf)	H6 K_{Ic} $MPa\sqrt{m}$	H7 K_{Ic} $MPa\sqrt{m}$	H8 K_{Ic} $MPa\sqrt{m}$	H9 K_{Ic} $MPa\sqrt{m}$	H10 K_{Ic} $MPa\sqrt{m}$
500	0.97	1.61	2.09	1.13	0.66
300	1.03	1.72	2.22	1.24	0.81
200	1.21	2.01	2.6	1.4	1.07
100	1.57	2.61	3.38	1.78	1.89

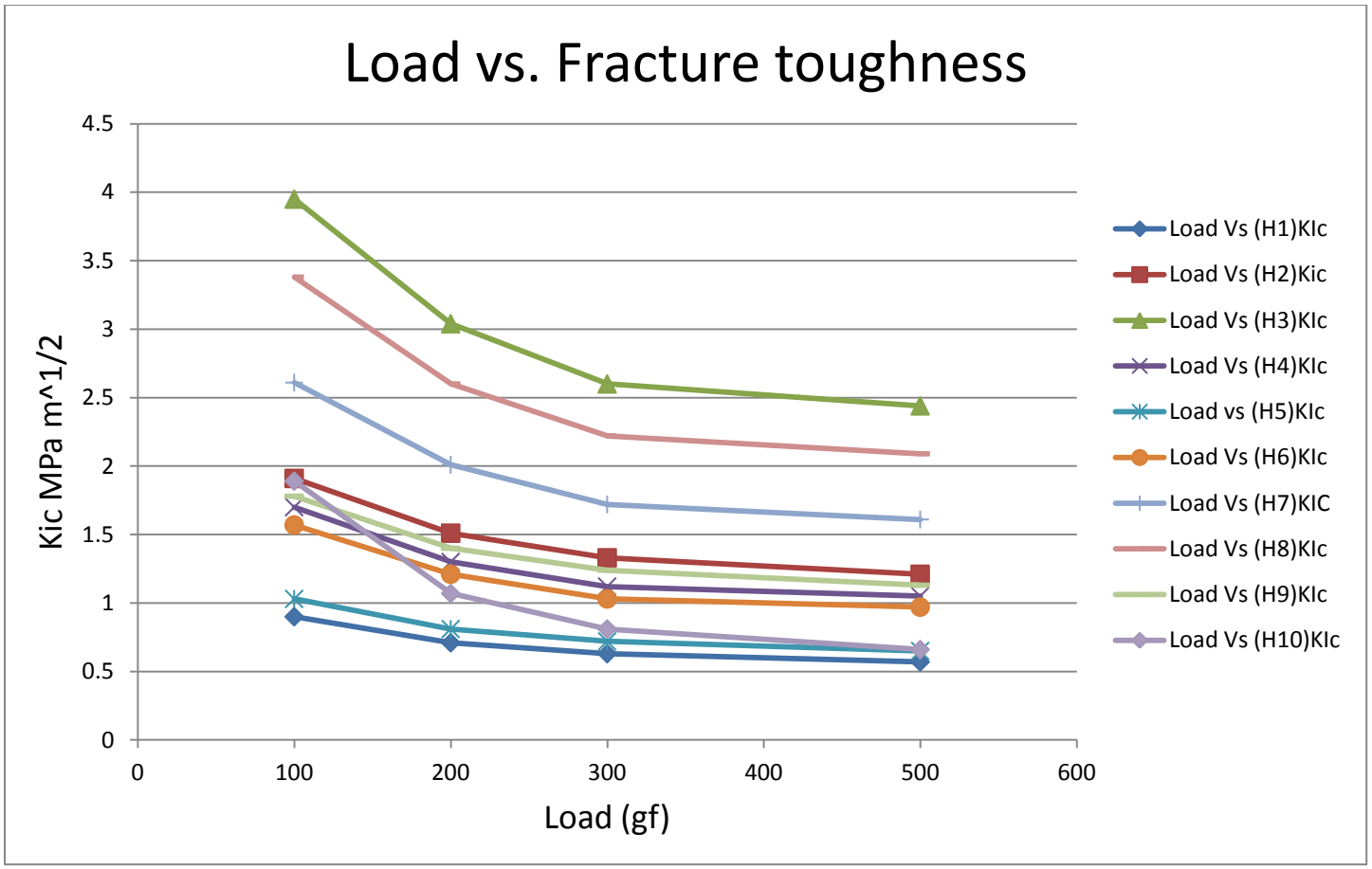

Figure 5-11 Graph of load vs. fracture toughness for different half-penny crack models, measured on 0.85 μm DLC thin film

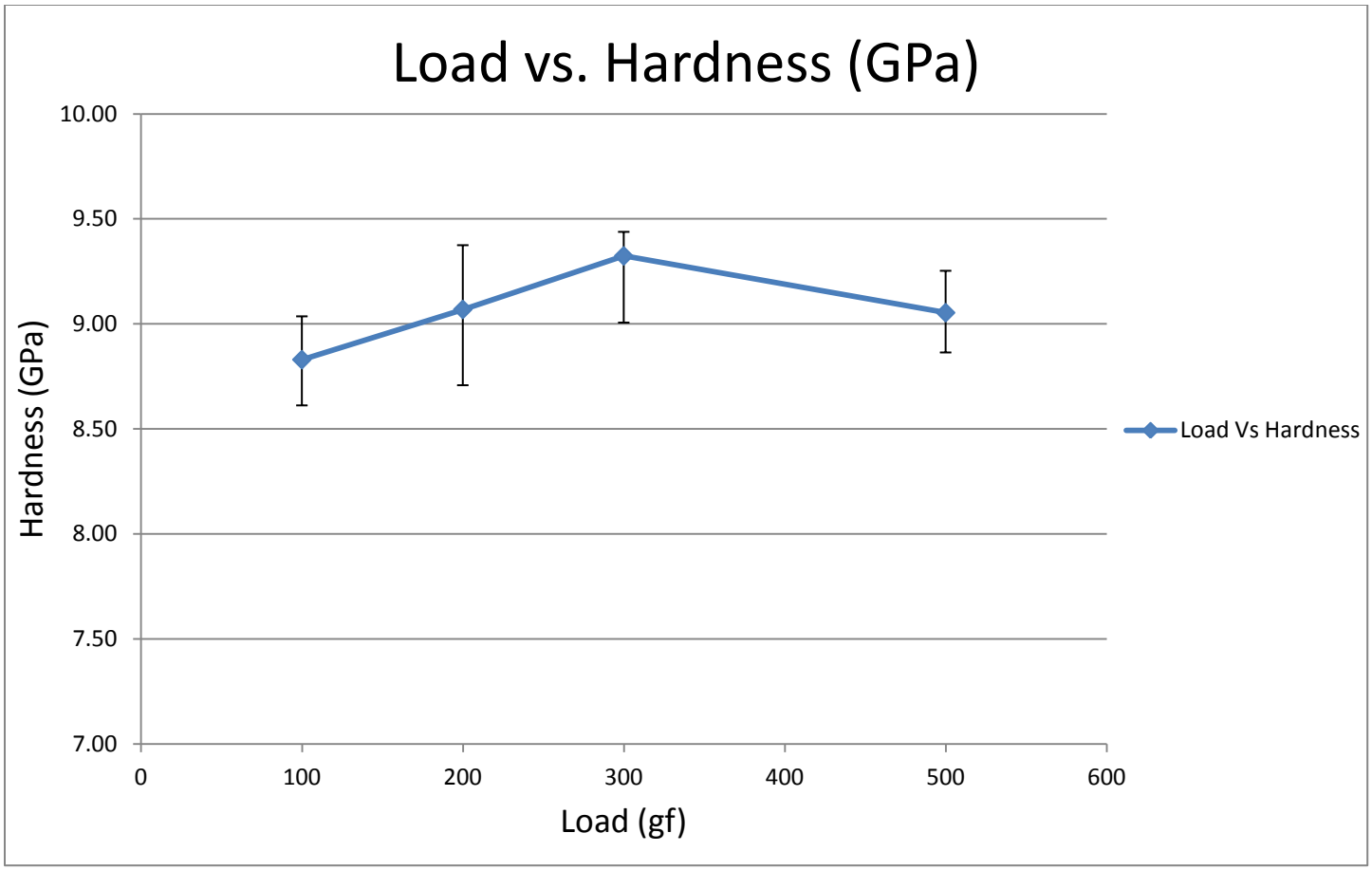

Figure 5-12 Graphs of load vs. hardness for 0.85 µm DLC thin film

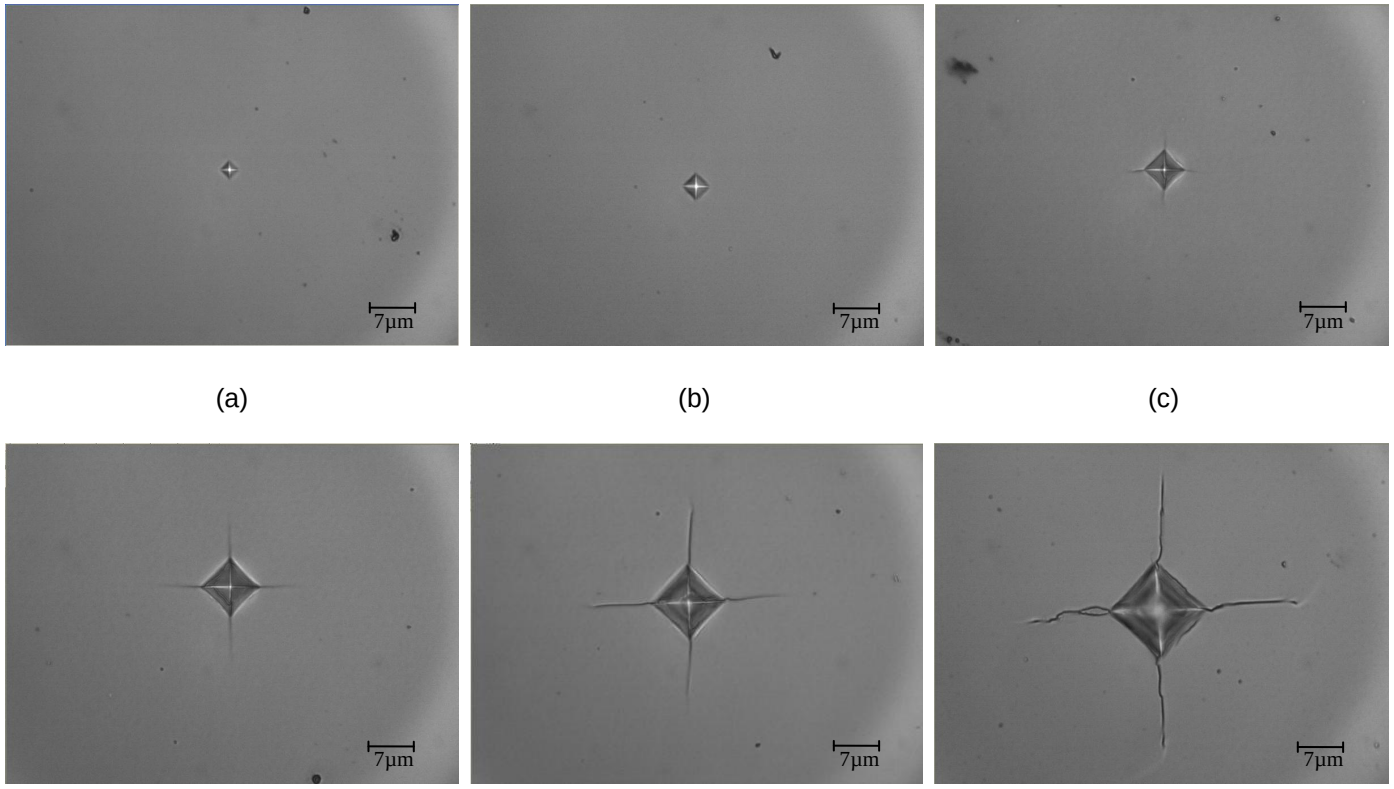

Figure 5-13 Vickers indentation image at 500x magnification on 0.85 μm DLC thin film, at load (a) 25 gf, (b) 50 gf, (c) 100 gf, (d) 200 gf, (e) 300 gf and (f) 500 gf

The same pattern is observed in 0.85 μm DLC thin film as it was seen in 0.4 μm DLC. Vickers indenter penetrated the DLC coating, resulting in influence of Si substrate in the result of hardness and fracture toughness. Hardness measured by indenting below 10% of DLC coating thickness using nanoindentation testing was 17.89 GPa and modulus of elasticity was 107.48 GPa.

All fracture toughness models from H1 to H10 for Vickers indenter failed to give correct fracture toughness. Figure 5-11 is showing that results of fracture toughness models are close to Si fracture toughness result due to influence of Si substrate in DLC fracture toughness measurement.

Load vs. hardness curve in figure 5-12 showed no major change in hardness throughout the load rage of 100 to 500gf. Microhardness testing result is higher in comparison to 0.4 μm because of increase in the coating thickness of DLC and less penetration of indenter in thin film.

Image of indentation on specimen surface are shown in figure 5-13. Cracking of DLC film does not occur at load below 100 gf. For the load range 100 to 500 gf no secondary cracks or buckling of thin film is observed.

5.6 Fracture Toughness Measurement of (100) Single Crystal Si using Cube-corner Indenter

Since Vickers indenter approach failed, cube-corner indenter was used for fracture toughness measurement. Load control and displacement control type of indentations were made by cube-corner indenter using nanoindenter. Initial analysis was made on (100) single crystal Si wafer and imaged by AFM. Indentation length and crack length are measured from the scanned AFM images of each indent. Using the load vs. displacement curve, hardness and modulus of elasticity are measured for all the indents.

Fracture toughness model C1, C2 and C3 are applied to measure fracture toughness using cube-corner tip. Fracture toughness results measured using different models at different loads are presented in table 5-5.

Table 5-5 Fracture toughness measurement of (100) single crystal Si using cube-corner indenter

Si wafer	
Thickness	0.34 mm
Poisson ration	0.22
Literature K_{Ic}	0.95 $MPa\sqrt{m}$

	Load control
	Displacement control

Material	Load (μN)	C1 K_{Ic} $MPa\sqrt{m}$	C2 K_{Ic} $MPa\sqrt{m}$	C3 K_{Ic} $MPa\sqrt{m}$
Si (100)	1380.68	0.93	1.55	1.40
Si (100)	1859.65	0.64	1.06	0.51
Si (100)	2500.13	0.67	1.11	0.49
Si (100)	5000.19	0.77	1.29	0.76
Si (100)	5000.16	0.76	1.27	0.75
Si (100)	5000.01	0.73	1.22	0.60
Si (100)	4999.82	0.61	1.01	0.50
Si (100)	5000.04	0.79	1.32	0.81
Si (100)	5000.13	0.77	1.29	0.79
Si (100)	6000.16	0.72	1.19	0.67
Si (100)	7000.23	0.64	1.07	0.51
Si (100)	7000.09	0.70	1.17	0.63
Si (100)	7999.54	0.70	1.17	0.57
Si (100)	8264.74	0.70	1.17	0.55
Si (100)	8500	0.61	1.01	0.43
Si (100)	8858.77	0.70	1.17	0.62
Si (100)	9000.27	0.70	1.17	0.58
Si (100)	9500.23	0.69	1.14	0.52

Comparison between different fracture toughness models using cube-corner tip at different loads are made in figure 5-14. Figure 5-15 shows scanned AFM images of different cube-corner indentations made on the specimen surface at different load.

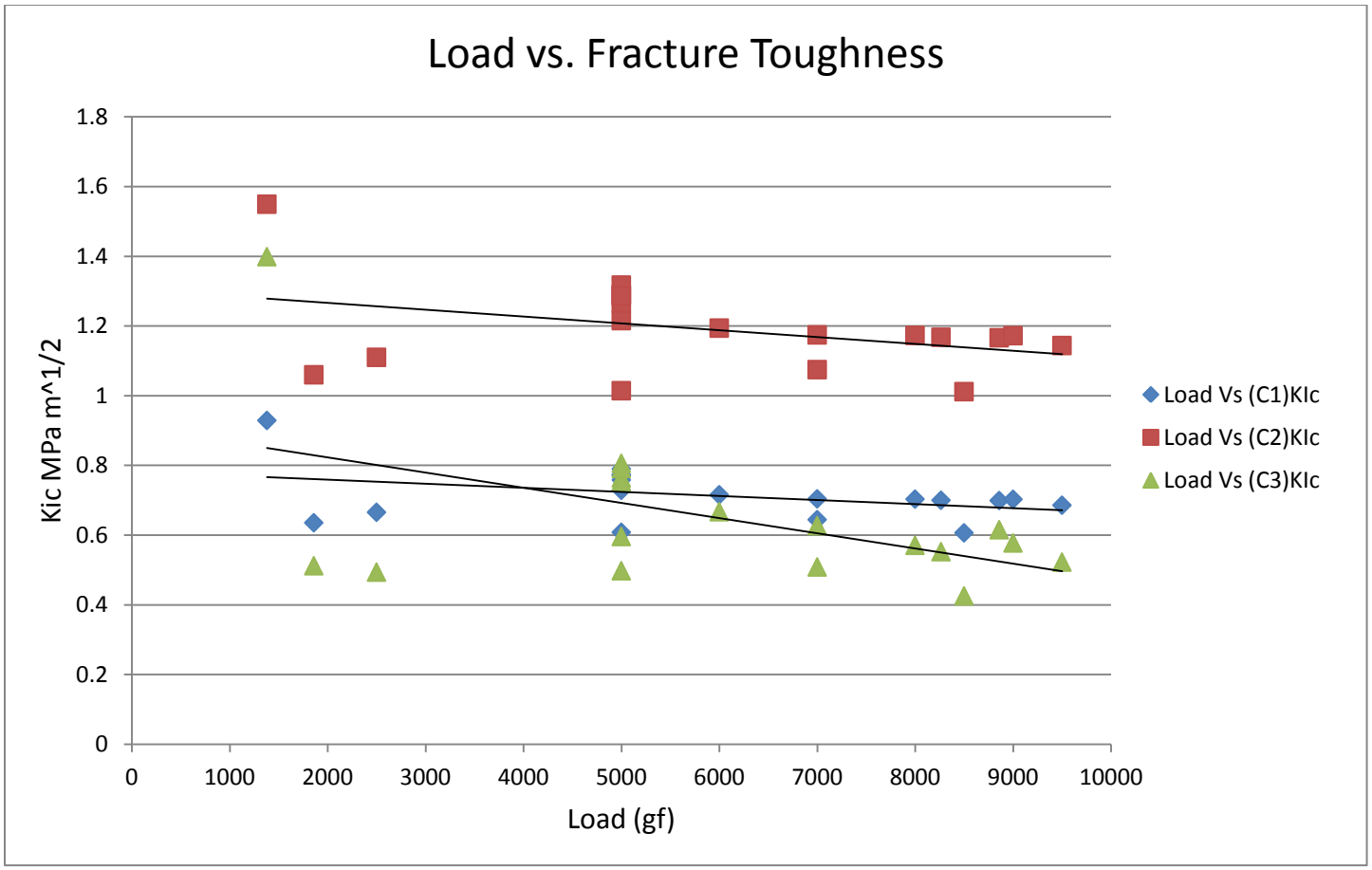

Figure 5-14 Graph of load vs. fracture toughness in single crystal Si using different model of cube-corner indenter

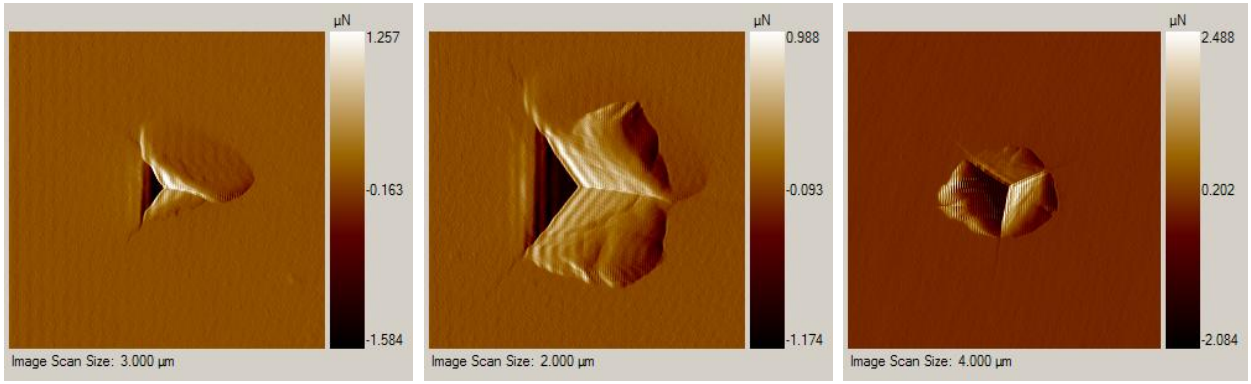

(a) (b) (c)

(d) (e) (f)

Figure 5-15 Nanoindentation images made by cube-corner indenter at load (a) 2500 µN, (b) 5000 µN, (c) 6000 µN, (d) 7000 µN, (e) 8500 µN and (f) 9500 µN

Fracture toughness measured in Si using Evans and Lawns (C1) and Laugier (C3) models show good agreement with standard results. However, Jang and Pharr (C2) gave much better result for Si. Graph of load vs. fracture toughness shown in figure 5-14 show variations in result at low load. Indentation fracture toughness result are accurate at load above 5000 μN. Multiple indent at 5000 μN were made at different loading rates and it shows that fracture toughness is independent of indentation loading rate.

Indentation images in figure 5-15 show that Si cracks under cube-corner indenter at load below 1000 μN and pileups around indenter area increases with increase in load.

Same approach for 0.4 and 0.85 μm DLC thin film showed no crack formation at load up to 9000 μN.

5.7 Fracture Toughness Measurement using Work Approach Model

A new approach is made in this model, for any given sample new tip empirical constant is measured to evaluate accurate fracture toughness. New empirical tip constant is generated in reference with standard material.

For all the nanoindentation carried out in Si, load vs. displacement graph was used to measure the total work done for loading a indenter and total work done during unloading a indenter and using the equation:

$$\frac{E}{H} = \frac{1}{1.07k} \times \frac{Wt}{Wu}$$

Comparing between standard hardness, modulus of Si and work done during loading & unloading we can measure constant k. Now substituting constant k in equation we can measure new tip constant λ

$$\lambda = \frac{\delta}{\sqrt{1.07k}}$$

Using modified Lawn equation (3.35) we measure fracture toughness of Si for individual indent using new modified tip empirical constant. Results of new fracture

toughness are presented in table 5-6. Figure 5-16 shows graph of load vs. fracture toughness for the given analysis.

$$K_{Ic} = \lambda \times \left(\frac{Wt}{Wu}\right)^{\frac{1}{2}} \times \left(\frac{P}{c^{1.5}}\right)$$

Table 5-6 Fracture toughness measurement using work approach method in (100) single crystal Si

Material	Load (µN)	W_t	W_u	C4 $K_{Ic}\, MPa\sqrt{m}$
Si (100)	1380.68	115990.59	162935.71	1.27
Si (100)	1859.65	207627.28	285718.84	0.85
Si (100)	2500.13	315516.95	478613.53	0.87
Si (100)	5000.19	1083857.14	1545905.50	1.05
Si (100)	5000.16	972537.60	1498078.30	0.97
Si (100)	5000.01	1005675.18	1512129.38	0.95
Si (100)	4999.82	1006729.72	1510163.17	0.84
Si (100)	5000.04	1005787.34	1523364.65	1.03
Si (100)	5000.13	1022272.56	1507226.72	1.04
Si (100)	6000.16	1388368.47	2088590.77	0.92
Si (100)	7000.23	1741881.75	2617377.48	0.84
Si (100)	7000.09	1759144.86	2648662.94	0.91
Si (100)	7999.54	2163017.22	3276547.38	0.89
Si (100)	8264.74	2571917.42	3177639.96	1.03
Si (100)	8499.62	2282679.32	3453529.06	0.83
Si (100)	8858.77	3244042.88	4006753.36	1.00
Si (100)	9000.27	2601044.41	3882326.04	0.94
Si (100)	9500.23	2857764.99	4233065.92	0.93
				Avg = 0.95

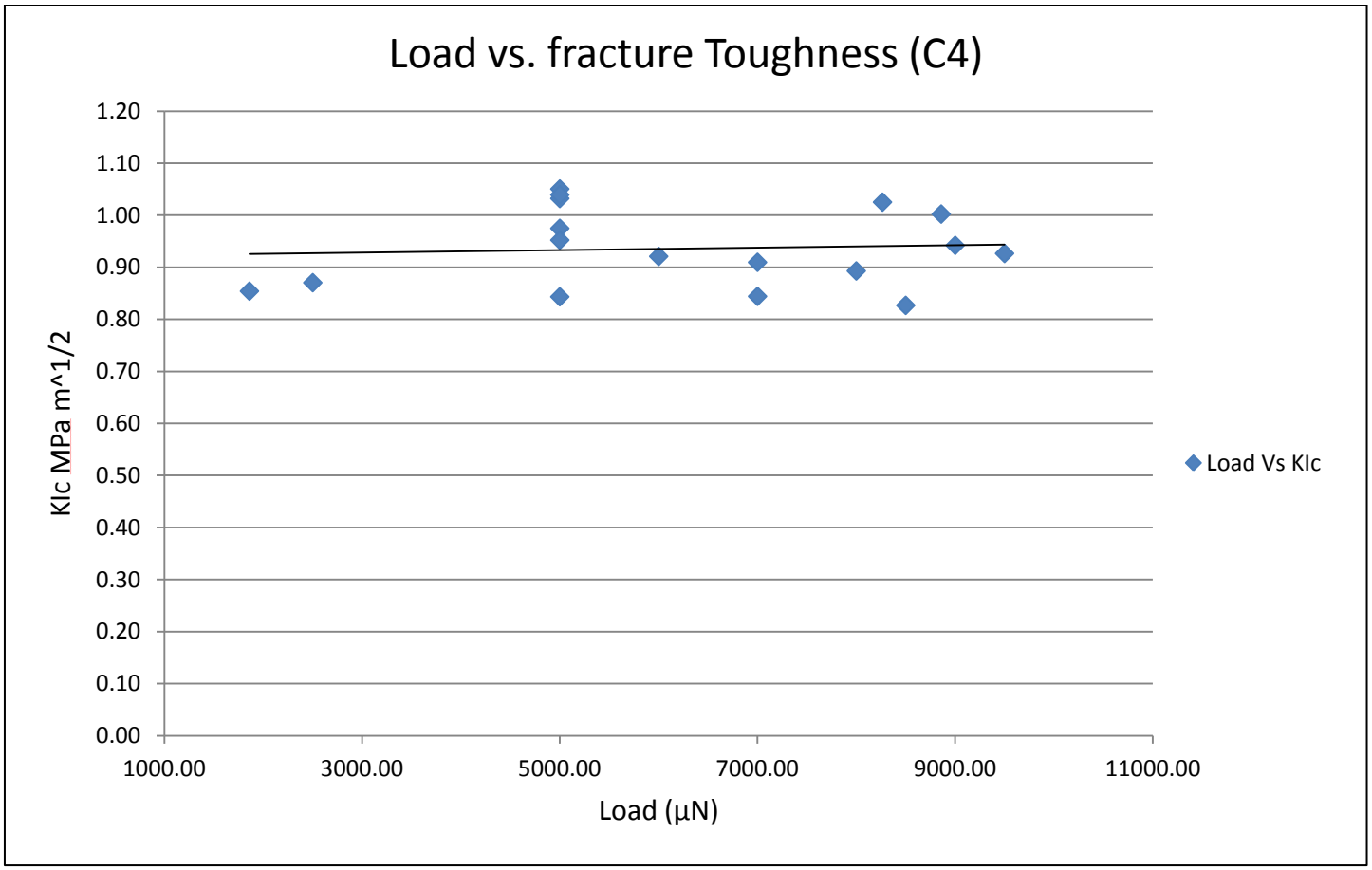

Figure 5-16 Graph of load vs. fracture toughness, measured using work approach model for single crystal Si

This model for measurement of fracture toughness show excellent agreement with the standard result of Si and the error in result is least. This method is more accurate for fracture toughness measurement because it modifies tip empirical constant with respect to specimen material type, similar to creating a calibration to eliminate tip error function.

However, this model is not applicable for DLC thin films, since there is no standard sample to compare the results. This model can be used successfully for measuring fracture toughness in brittle bulk materials.

5.8 Fracture Toughness Measurement using Energy Release Model

Final approach was made in 0.4 μm DLC to crack thin film using cube-corner indenter, achieved at load of 9300 μN and loading rate of 45 nm/s. Figure 5-17 show clear linear crack generated on the DLC thin film surface. It was a displacement controlled indentation made at 450 nm displacement.

However, it was not possible to crack 0.85 μm DLC, even at load 10000 μN which is the machine limit.

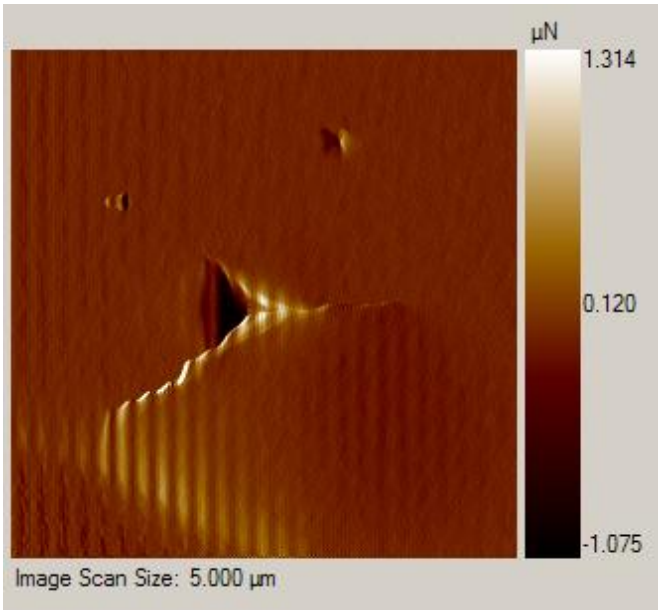

Figure 5-17 Cube-corner indentation on 0.4 μm DLC thin film

A clear step is observed in the figure 5-18 of load vs. displacement curve at 9170 μN. This step shows strain energy released during the cracking of DLC thin film. This energy released during the cracking was measured by measuring the area of plateau.

Fracture toughness of 0.4 μm DLC thin film is measured using fracture toughness model (C5) for cube-corner indenter in table 5-7. This result in table 5-7 is found to be in good agreement with other literature values.

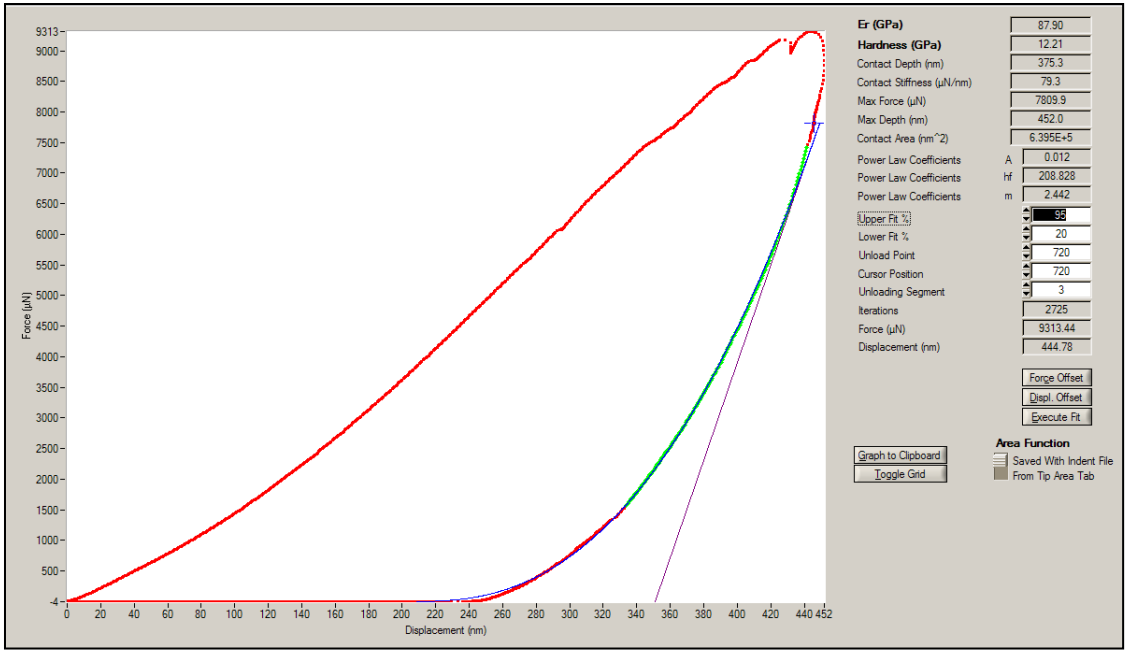

Figure 5-18 Load vs. Displacement curve for 0.4 µm DLC thin film

Table 5-7 Fracture toughness measurement using strain energy release model

Material	Load (µN)	Modulus of E (GPa)	Hardness (GPa)	Average Crack length (µm)	Coating thickness (µm)	U (µNm)	(C5) K_{Ic} $MPa\sqrt{m}$
0.4µm DLC film	9313.44	115.6	18.345	0.72	0.4	1.001	8.196

5.9 Summary of Results

Two types of indentation technique are used for characterization of fracture toughness. First indentation technique is microhardness testing using Vickers indenter. Ten different fracture toughness measurement models are applied and were found to be suitable for only brittle materials. DLC thin films below 1 μm thickness did not give good result of fracture toughness measurement. This was mainly because, at given load Vickers indenter penetrated DLC thin film layer and approached Si substrate. As a result fracture toughness result of thin film is similar to Si K_{Ic} result.

Second indentation technique used was nanoindentation testing. Using cube-corner tip all samples are indented at lower load, with lesser penetration of indenter tip. This technique was found to be more accurate for fracture toughness measurement compared to microhardness testing. Five different models are used for fracture toughness characterization under nanoindenter. Model C1, C2, and C3 are suitable for brittle material however, cube-corner did not generate any cracking on the DLC thin film in this case. Model C4 was found to be the most suitable method for fracture toughness measurement, since it was very accurate. Model C4 is based on calibration of tip empirical constant which requires a standard sample, this is not possible to find in DLC.

Model C5 is the most suitable for fracture toughness measurement of DLC thin film. It measures the strain energy released from load vs. displacement curve and corresponding it with DLC crack length gives a very good result. 0.4 μm DLC cracked at load 9300 μN, using the load vs. displacement curve strain energy was measured to characterize fracture toughness. However, for 0.85 μm DLC did not crack at load above 10000 μN. It may be possible to evaluate fracture toughness if machine had capacity to apply high load of 30000 or 40000 μN.

Chapter 6

Conclusion

1) Tip empirical constant has $\pm 25\%$ error which leads to an inherent uncertainty in the measured fracture toughness.
2) Vickers indenter can be a very reliable technique for brittle material fracture toughness measurement; however one also needs nanoindentation for modulus of elasticity measurement.
3) Vickers indenter fracture toughness results are not reliable for DLC thin film materials.
4) Different brittle materials require different fracture toughness model for fracture toughness measurement.
5) Without exceeding 10% of film thickness if we measure fracture toughness, we might achieve true result.
6) Secondary cracks and buckling of thin film generate error in fracture toughness measurement.
7) Cube-corner indenter is more reliable for brittle material as well as thin films, as they result in larger stress concentration leading to fracture of film at lower load.
8) Work approach model is the most reliable model for fracture toughness measurement in brittle materials, however it requires suitable calibration sample.
9) Most suitable fracture toughness measurement model for thin film is strain energy release model.

References

[1] J. Robertson, Diamond-Like Amorphous Carbon, Material Science and Engineering Reports: A Review Journal, Vol. 37, (2002) 129-281

[2] M. Nastasi, P. Kodali, K. C. Walter, and J. D. Embury, R. Raj, Y. Nakamura, Fracture Toughness of Diamond like Carbon Coatings, Journal of Materials Research, Vol. 14, No. 5 (May 1999) 2173-2180

[3] K. I. Schiffmann, Determination of Fracture Toughness of Bulk Materials and Thin Films by Nanoindentation: Comparison of Different Models, Philosophical Magazine, Vol. 91, Nos. 7–9, 1–21 (March 2011) 1163–1178

[4] Y. Feng, T. Zhang and R. J. Yang, A Work Approach to Determine Vickers Indentation Fracture Toughness, Journal of the American Ceramic Society, Vol. 94, (Jan 2011) 332–335

[5] D. Chicot, A. Pertuz, F. Roudet, M. H. Staia and J. Lesage, New Developments for Fracture Toughness Determination by Vickers Indentation, Materials Science and Technology Journal, Vol. 20, (July 2004) 877-888

[6] Nanoindentation by Anthony C. Fischer-Cripps, Springer publication, Third Edition

[7] K. R. Morasch, Nanoindentation Induced Thin Film Fracture, Thesis, Washington State University, (May 2005)

[8] Manufacturing Engineering and Technology by K. Serope and S. Steven, McGraw Hill, 2005, Ch. 2, pp. 76, 78-79.

[9] J. J. Kruzic and R. O. Ritchie Determining the Toughness of Ceramics from Vickers Indentations Using the Crack-Opening Displacements: An Experimental Study, Communications of the American Ceramic Society, Vol.86, No. 8 (2003) 1433–1436

[10] H. Hertz, Contact of Elastic Solids, Hertz's Miscellaneous Papers. London: Macmilllan & Co,(1896)

[11] Boussinesq's Problem for a Rigid Cone by Sneddon Ian N, Proceedings of the Cambridge Philosophical Society, Vol. 44, No. 4 (1948) 492

[12] W. C. Oliver, G. M. Pharr, An Improved Technique for Determining Hardness and Elastic Modulus using Load and Displacement Sensing Indentation Experiments, Journal of Materials Research, Vol. 7, (1992)

[13] A. G. Evans and E. A. Charles, Fracture Toughness Determinations by Indentation. Journal of American Ceramic Society, Vol. 59, (1967) 371–372

[14] B. R. Lawn, A.G. Evans and D. B. Marshall, Elastic/Plastic Indentation Damage in Ceramics: the Median/Radial crack system, Journal of American Ceramic Society, Vol. 63, (1980) 574-581

[15] G. Strnad and L. J. Farkas, Improving the Accuracy of low-load Vickers Microhardness Testing of Hard Thin Films, Procedia Technology, Vol. 12, (2014) 289-294

[16] R. F. Cook and G. M. Pharr, Direct Observation and Analysis of Indentation Cracking in Glasses and Ceramics, Journal of American Ceramic Society, Vol.73 (1990) 787-817

[17] H. Hertz, On the contact of elastic solids, J. Reine Angew, Maths, Vol. 92, (1881) 156-171

[18] A. G. Evans and E. A. Charles, Fracture Toughness Determinations by Indentation, Journal of American Ceramic Society, Vol.59, (1976) 371-372

[19] H. Hertz, On Hardness, Verh.Ver.BefÖrderung Gewerbe Fleisses, Vol. 61, (1882) 410

[20] H. R. Lawn and E. R. Fuller Equilibrium Penny-like Cracks in Indentation Fracture, Journal of American Ceramic Society, Vol.10, (1975) 2016–2024

[21] R. Spiegler, S. Schmadder & Lorenz S. Sigl, Fracture Toughness Evaluation of WC-Co Alloys by Indentation Testing, Journal Of Hard Materials, Vol. 1, No. 3 (1990) 147-158

[22] G. R. Anstis, P. Chantikul, B. R. Lawn and D. B. Marshall, A Critical Evaluation of Indentation Techniques for Measuring Fracture Toughness – I. Direct Crack Measurements, Journal of American Ceramic Society, Vol. 9, (1981) 533-5413

[23] K. Niihara, R. Morena, and D. Hasselman, Evaluation of Kic of Brittle Solids by the Indentation Method with Low Crack-to-Indent ratios. Journal of American Ceramic Society, Vol. 1, (1982) 13–16

[24] K. Niihara, A Fracture Mechanics Analysis of Indentation-Induced Palmqvist Crack in Ceramics, Journal of American Ceramic Society, Vol. 2, (1983) 221–223

[25] M. T. Laugier, Journal of Material Science, Vol. 4, (1985) 1539-1541

[27] A. G. Evans and T. R. Wilshaw, Quasi-static Solid Particle Damage in Brittle Solids – I. Observations, Analysis and Implications. Acta Materialia, Vol. 24, (1976) 939–956

[28] D. K. Shetty, I. G. Wright, P. N. Mincer, and A. H. Clauer. Indentation Fracture of WC-Co Cermets, Journal of Material Science, Vol. 20, (1985), 1873–1882

[29] T. Zhang, Y. Feng, R. Yang and P. Jiang. A Method to Determine Fracture Toughness using Cube-corner Indentation, Scripta Materialia, Vol. 62, (2010) 199–201

[30] J. I. Jang and G. M. Pharr, Acta Materialia, Vol.56, (2008) 4458

Biographical Information

Ronaksinh Navalsinh Parmar was born on 6 November, 1991 in Ahmedabad, Gujarat, India. He attended N.R. high school and received his Bachelor of Engineering in Metallurgical Engineering from Gujarat Technological University in 2013. During his undergraduate program, his water atomization model project was awarded with best undergraduate project of the year in Metallurgy department.

Since 2014, he started to pursue Master degree in Material Science and Engineering at University of the Texas at the Arlington. Here he researched on "Characterization of Fracture Toughness in Diamond Like Carbon Thin Films and Coatings" and received his Master of Science in Materials Science and Engineering in August of 2015.

His Hobbies are quad copter modeling and 3D printing.